Numerical investigation of the behavior of precast concrete segmental columns subjected to vehicle collision

Tin V. Do[1], Thong M. Pham[2], and Hong Hao[3]

Abstract

This study numerically investigates the response of precast concrete segmental columns with unbonded prestress tendons subjected to vehicle collision. Numerical models are developed using LS-DYNA and validated against experimental tests. The validated model is then used to perform intensive numerical simulations to analyze the effectiveness of prestressing level, number of segments, concrete strength, and vehicle velocity on the behavior of precast segmental concrete columns. The numerical results have shown that the effect of the initial prestressing level and the number of segments are marginal on the impact force time history but significant on the residual displacement and the damage of the column. Better self-centering capacity as well as smaller lateral displacement can be achieved on segmental columns by reducing the number of column segments and increasing the prestress level. In addition, the height-to-depth ratio of a concrete segment should be smaller than two in order to minimize an undesirable local damage at the rear side opposite the impact point. Varying concrete strength from 20 MPa to 80 MPa shows an unnoticeable change of the impact force but its effects on mitigating the damage of the columns are considerable. Last but not least, increasing the impact velocity does not always increase the peak impact force of a segmental column. It is

[1]PhD Scholar, Center for Infrastructural Monitoring and Protection, School of Civil and Mechanical Engineering, Curtin University, Kent Street, Bentley, WA 6102, Australia. Email: tin.v.do@postgrad.curtin.edu.au

[2] Research Fellow, Center for Infrastructural Monitoring and Protection, School of Civil and Mechanical Engineering, Curtin University, Kent Street, Bentley, WA 6102, Australia. Email: thong.pham@ curtin.edu.au

[3]John Curtin Distinguished Professor, Center for Infrastructural Monitoring and Protection, School of Civil and Mechanical Engineering, Curtin University, Kent Street, Bentley, WA 6102, Australia (corresponding author). Email: hong.hao@curtin.edu.au

recommended that both the peak impact force and impulse should be taken into consideration in the analysis and design of segmental columns against vehicle impact.

Keywords: Precast concrete segmental columns; prestress tendons; vehicle collision; numerical simulation; contact algorithm;

1. Introduction

Precast concrete segmental columns (PCSCs) have been more intensively studied in recent years owing to their many advantages compared to conventional cast-in-place concrete structures [1, 2]. These include significantly reducing the construction duration, enhancing on-site efficiency, diminishing environmental impacts, improving work-zone safety, and better construction quality control in a prefabrication workshop. Apart from the mentioned benefits, precast segmental elements prepared in the factory also offer a feasible solution to applications of new materials such as ultra-high performance concrete, fiber reinforced concrete which usually requires temperature control or careful mixing. Although PCSCs have been widely used over the world, studies on their performance and behavior under impact loading such as vehicle collision are very rare [3-5]. With the rapid development of cities and highway networks around the world as well as the increase of traffic in urban areas, bridge columns and ground story columns of buildings are vulnerable to vehicle collision (Fig.1). The knowledge on the behavior of PCSCs under vehicle impact are, therefore, necessary and crucial for their applications in construction.

(a) Chatfield Road Bridge (b) Tancahua Street Bridge, Texas

Fig. 1. Truck accident [6].

Recent knowledge on PCSCs under dynamic lateral loadings focuses mainly on their seismic capability. Many studies have reported the behavior and failure modes of PCSCs under cyclic

loading for their applications in high-seismicity regions [2, 7-11]. Pros and cons of PCSCs in resisting seismic loading as compared to traditional monolithic columns have been therefore presented and possible design improvements were suggested. Comparing with many studies on PCSCs under seismic loading, studies on the impact-resistant capacity of PCSCs are very limited with only three studies can be found in the open literature [3-5, 12]. Recently, the responses of PCSCs under vehicle collision are studied using numerical simulation by Chung et al. [3]. In that study, a numerical model of a PCSC which was 16.25 m in height and 2.3 m in diameter subjected to an 8-ton-vehicle impact was built. The dynamic performances of PCSCs were compared to a cast-in-place monolithic column. Resulting from the relatively smaller stiffness, the maximum displacement of the PCSC was higher than the conventional monolithic column. A relative lateral slip was also observed at the bottommost joint between the foundation and the first concrete segment which also contributed to the lateral displacement. The slip between the bottom segment and foundation raised a concern of using PCSCs in resisting impact forces. However, in the latter numerical model, modeling of the prestress tendons was not mentioned in the study and thus the capability of prestress tendons in controlling the maximum and residual displacement of the column was probably ignored. The accuracy of the numerical model was not validated either. Since no severe damage or failure was observed due to the large size of the column modeled compared to the relatively small impact energy of the considered vehicle, the impact behavior of the column with local concrete damage around the impacting point, as well as the large deformation and failure were not considered in the latter model.

On the other hand, Zhang et al. [4] used a pendulum impact testing system and performed impact tests of scaled PCSCs. The PCSCs post-tensioned with unbonded prestress tendon were experimentally investigated under progressively increasing impact velocities and the results were then compared with a reference monolithic column. It was observed that under the same

initial impact conditions, the segmental joints opened, i.e., rocking of segments, to dissipate energy while the monolithic column showed concrete tensile cracks. Therefore, the PCSCs showed better impact-resistant and self-centering capacity than those of the counterpart. The effectiveness of the segment number was also discussed in the latter experimental study. The more segments in PCSCs, the more columns' flexibility was observed, resulted from joint openings. As a result, smaller peak impact force and more energy dissipation were observed. Zhang et al. [4] observed the similar problem reported in the previous numerical study that shear slips occurred between the impacted segment and its adjacent segments. To improve the shear resistance capability of PCSCs, unreinforced concrete tower shear keys were utilized in a subsequent study in segments of PCSCs to resist lateral impact forces by Zhang et al. [5]. By introducing tower concrete shear keys, under the same loading condition, the column with concrete shear keys significantly reduced the relative displacement between segments by about 70% as compared to the columns without shear keys. However, it was also observed that large concrete shear keys led to increasing stress concentration within the segment and resulted in more severe damage observed in the concrete segment subjected to impact. Hao et al. [12] carried out experimental tests on a new design of dome shear keys between the concrete segments in the latest pendulum impact test. The testing results indicated that although the tower-shear-key column and the dome-shear-key column observed a similar concrete damage under similar small impact loading, the latter managed to survive and carried the top structures while the former was totally destroyed at the highest impact load. However, the dome-shear-key column showed a higher residual displacement at the column mid-height compared to the tower-shear-key column. Based on the impact performances of the segmental column with shear keys, it is found that the concrete shear keys significantly reduce the column lateral displacement, increase the column stability, and shear resistances of the segmental columns but some limitations are still exist, i.e. stress concentration at the key corner (tower shear keys),

94 easily slippage (dome shear keys). Therefore, further improvements on shear key design are
95 needed and are under investigation by the authors.
96 From the above review, it is clear that a calibrated numerical model that properly considers the
97 influences of prestress level in the tendons on the responses, failure modes, and local damage
98 of columns needs be developed to realistically predict the performance of segmental columns
99 subjected to vehicle impact. The model can also be used to study the influences of the varied
100 number of segments, concrete strength, and impact velocities on the responses of the segmental
101 columns.
102 In this paper, a detailed 3D model is built with the commercial software LS-DYNA [13]. The
103 accuracy of the numerical model is then verified against the available experimental impact
104 testing results by Zhang et al. [4]. The performances of segmental precast concrete columns
105 under vehicle collision are then investigated. The main objectives of this study are as follows:
106 (1) present an effective modelling method of the responses of PCSCs under impact forces; (2)
107 numerically investigate the responses of PCSCs under vehicle collision; (3) carry out a
108 parametric investigation of the effectiveness of different parameters including prestress level,
109 number of segments, concrete strength on the behavior of PCSCs to resist vehicle impact with
110 different velocities.

111 ## 2. Numerical model calibration

112 ### *2.1. Available impact test*

113 The experimental tests on PCSCs by Zhang et al [4] as illustrated in Fig. 2 are used to calibrate
114 the developed numerical model. The test results of the PCSC with five segments are presented
115 and compared with the numerical results. The designs of the segmental column and the impact
116 tests are briefly described in this section.

117 Fig. 2 shows the schematic view of the specimen and the experimental pendulum impact test
118 setup. The overall dimensions of the testing column were 800 mm in height and 100 mm x 100
119 mm in cross-section area. The column consisted of five precast concrete segments with 160 mm
120 in height of each segment. A 15 mm diameter hole was left at the center of each segment for
121 the prestress tendon when casting the segments. A footing of 140 mm deep and 400 mm x 400
122 mm in cross – section area was built to connect the segmental columns to the laboratory strong
123 floor. A constant weight of 288 kg consisting of 400 mm x 400 mm x 450 mm (L x W x H)
124 concrete block and 5 pieces of 23 kg steel plates was firmly fixed to the top of the column. The
125 compressive strength and flexural tensile strength of concrete material were 34 MPa and 5 MPa,
126 respectively.
127 Each segment was reinforced with four 6 mm diameter longitudinal bars (f_y = 500MPa) which
128 were discontinuous between the segments. Four 4 mm diameter ties (f_y = 300MPa) were utilized
129 as shear reinforcements. The bottommost segment is connected to the footing by two 6 mm
130 diameter starter bars. Seven–wire strands with 9.3 mm in diameter and of grade 1860 MPa were
131 used as a prestress tendon with the barrel anchored inside the footing and the wedge placed on
132 the top of steel plates. After finishing the installation of the column, a 30 kN force which was
133 equivalent to 23.7% of the yielding capacity of the tendon was applied.
134 The pendulum impact testing system consisted of a steel frame, a pendulum arm, and a steel
135 impactor. Two pieces of solid steel impactor with a total mass of 300 kg were connected to
136 strong steel frame through the 2.8 m long pendulum arm. The pendulum impactor was lifted to
137 a designated angle and then released to impact the center of column in each test. The impact
138 velocity was progressively increased in the test by lifting the pendulum to a higher position
139 until the collapse of the column specimen. The angles were 2.5 degrees, 7 degrees, and 15
140 degrees which corresponded to the impact velocity of 0.23 m/s (Impact 1), 0.64 m/s (Impact 2),
141 and 1.37 m/s (Impact 3).

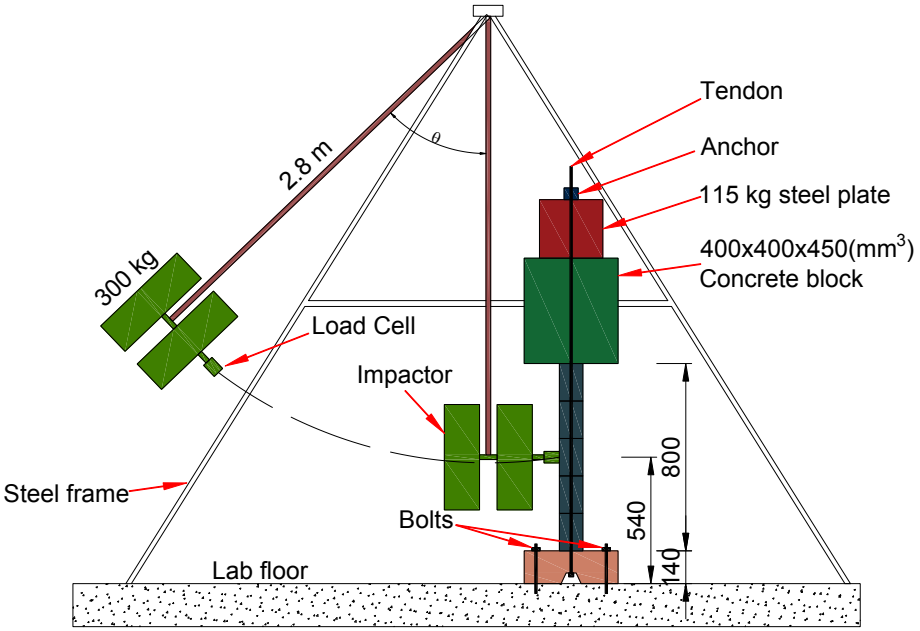

Fig. 2. Schematic view of the pendulum impact test setup

2.2. Numerical simulation

2.2.1. Method of pre-stressing load

To apply the prestress load in a numerical model, many methods have been introduced in the literature. Li et al. [14] modeled prestress on PSCCs subjected to blast load by applying a constant compressive load on concrete surface and a tensile force in the tendon. This pre-loaded force is applied by using LS-DYNA keyword card *LOAD_SEGMENT_SET with the pre-stressing load being unchanged during the whole response duration. Although this approach is easy and straightforward, it neglects the effect of tendon deformation and the associated change in the prestress level in concrete structures during the dynamic response. Under intensive dynamic loading, the tendon is expected to experience large elongation because of large deformation of columns, which leads to an increase in the compressive force on structures. The latter method is not able to model the prestress variation during the dynamic response of the structure. Chen et al. [15] modelled the response of prestressed concrete beam subjected to

157 blast loading by using numerical simulation. The prestress on concrete beam was created by
158 applying the initial hogging deformation at the midspan of the beam. From the static analysis,
159 the relationship between the prestress force and the initial hogging deflection of reinforced
160 concrete (RC) beam is determined, which is applied to modify the beam initial geometry
161 through the implicit analysis by using ANSYS. The response of the beam subjected to blast
162 loading is then analyzed using the explicit calculation in LS-DYNA. This method can solve the
163 drawback of the former method reviewed above because the prestress variations are modelled
164 with the beam deformation. However, the process of applying the initial hogging geometry to
165 the beam model is tedious and time consuming. Moreover the initial deflection of RC beam is
166 not straightforwardly calculated either if the prestress is not horizontal and uniform across the
167 beam.
168 To overcome these problems, a temperature-induced shrinkage in pre-stressing strand offers a
169 feasible solution [16, 17]. In this approach, the *DYNAMIC RELAXATION (DR) option is
170 used to create the stress initialization process. The DR feature allows implemention of an
171 explicit analysis before transferring the results to an implicit simulation [13]. The ratio of
172 current-to-peak distortional kinetic energy from applied prestress load will be checked every
173 250 cycles. The DR phase will terminate when the distortional kinetic energy has sufficiently
174 reduced and the convergence factor is smaller than the defined tolerance value. The DR results
175 then automatically proceed to the transient analysis phase. To optimize the converged results,
176 the convergence tolerance can be defined by users (default value: 10^{-3}). The smaller value of
177 the tolerance results in converged solution closer to the steady stage but it required longer
178 computing time. In this study, the value of convergence tolerance is used at 10^{-5}. It should be
179 noted that a damping coefficient must be designated in the DR to achieve converge of the DR
180 results [13]. For concrete structures, the damping coefficient normally ranges from 0.02 to 0.05

[18-20]. As a result, the value of 0.05 is used for the damping coefficient to converge the DR results.

The LS-DYNA material card *MAT_ELASTIC_PLASTIC_THERMAL (MAT_004) is used for defining the relation between material property of tendon and temperature. Following this material, *LOAD_THERMAL_LOAD_CURVE card is used for defining the time dependence of temperature through initial phase and explicit phase. LS-DYNA requires two time-temperature curves for this option. The first curve is for dynamic relaxation phase (implicit analysis), where the temperature decreases suddenly from the reference temperature to the defined temperature and then levels off. The second time-temperature curve is kept constant for an explicit phase. An example of these two curves is shown in Fig. 3.

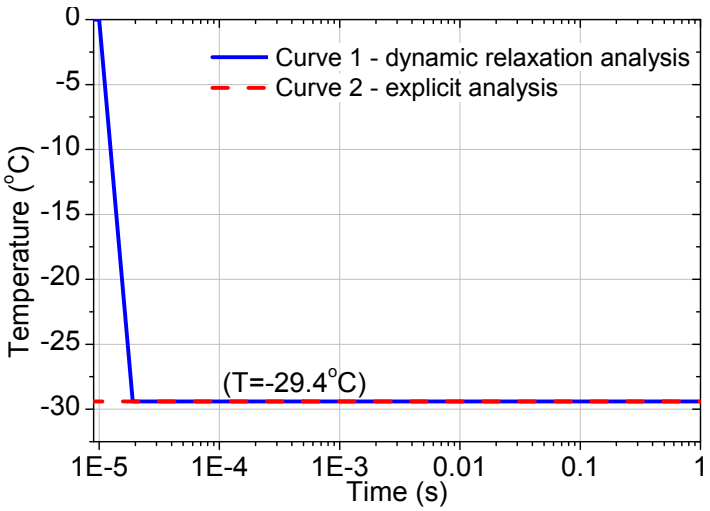

Fig. 3. Temperature versus time curves

To better understand this prestress method, a simple concrete block and a tendon located at the middle are employed as an example to illustrate the procedure. Fig. 4a shows the un-bonded tendon is placed inside the concrete block with the top anchor being connected to the tendon for creating the pre-stressing load. The contact algorithm named AUTOMATIC_SURFACE_TO_SURFACE (ASTS) is used to define a contact between the anchor and the concrete block. With this feature when the tendon is shortened by the dropping of temperature, the tensile force is created in the tendon and the compressive force is generated

simultaneously in the concrete block. The total deformation of concrete and tendon is equal to the deformation of the tendon when the temperature drops without any restraint, which is illustrated by Fig. 4b.

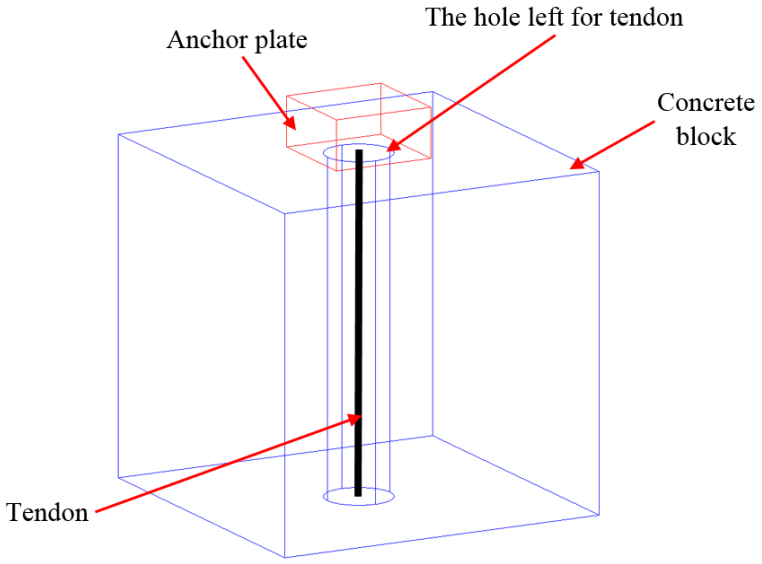

(a) Single concrete element for un-bonded prestress tendon

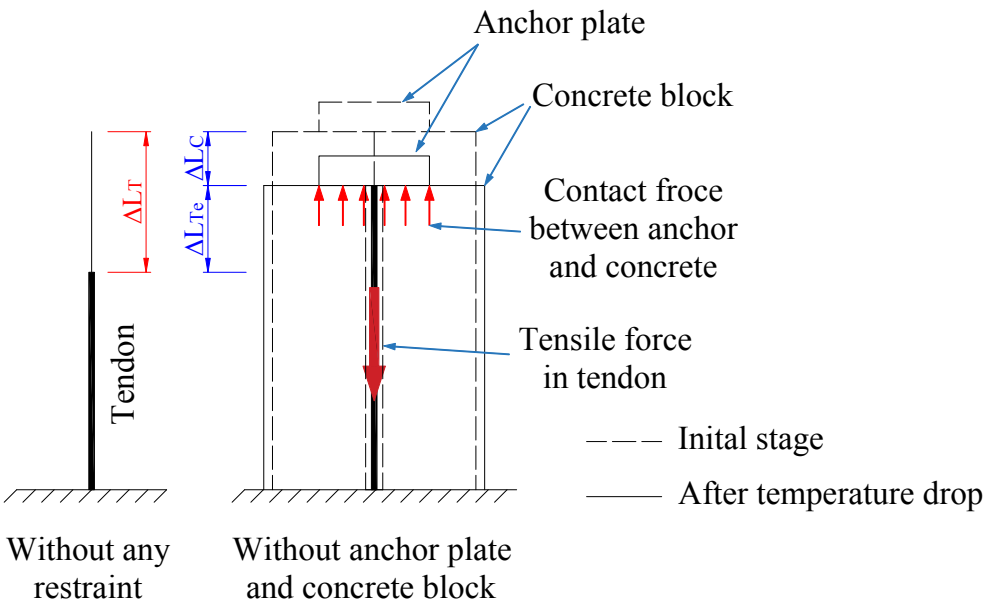

(b) Deformation of tendon when temperature drops

Fig. 4. Illustration of the proposed method for application of un-bonded prestress in concrete structures

The deformations of the concrete block and tendon can be equated as follows:

$$\Delta L_C + \Delta L_{Te} = \Delta L_T \tag{1}$$

where ΔL_C is the shortening of the concrete element, ΔL_{Te} is the elongation of tendon element, and ΔL_T is the shortening of the tendon when the temperature drops without contact force. The compatibility of strain between concrete and tendon is therefore written by Eq. (2a).

$$\varepsilon_c + \varepsilon_{Te} = \varepsilon_T \tag{2a}$$

or

$$\frac{f}{A_c E_c} + \frac{f}{A_s E_s} = \Delta T \times \alpha \tag{2b}$$

where ε_c is the strain of the concrete, ε_{Te} is the strain of the tendon when the temperature drops with anchor plate and concrete block, ε_T is the strain of the tendon when the temperature drops without any restraints, f is the pre-stressing force, A_s and E_s are cross section area and elastic modulus of tendon, respectively, A_c and E_c stand for the corresponding measures of concrete, ΔT is the change of temperature, and α is the thermal expansion coefficient of tendons.

From the expected pre-stressing force, the change of temperature, ΔT , can be obtained by the following equation:

$$\Delta T = \frac{f}{\alpha}\left(\frac{1}{A_c E_c} + \frac{1}{A_s E_s}\right) \tag{3}$$

2.2.2. Constitutive model of materials

There are various types of material models available for modelling concrete material subjected to blast and impact loads in LS-DYNA such as *MAT_WINFRITH_CONCRTE (MAT_084-085), *MAT_CSCM_CONCRETE (MAT_159), *MAT_CONCRETE_DAMAGE (MAT_072), and *MAT_CONCRETE_DAMAGE_REL3 (MAT_072R3), etc. In this study, the MAT_072R3 material model is selected for the simulation of concrete material where

strain-rate effect, plasticity, and shear failure damage are taken into consideration. The accuracy of this model in simulating the performance of concrete structures under extreme dynamic loading has been verified in many previous studies, e.g. [14, 21, 22]. The unconfined compressive strength of concrete is an important input parameter of this material model when the remaining parameters can be generated automatically from that value. It is worth mentioning that the generated material parameters can also be modified by users. In this study, the unconfined compressive strength of concrete material is 34 MPa.

For the steel reinforcements, an elastic-plastic material model named *MAT_PIECEWISE_LINEAR_PLASTICITY (MAT_24) is utilized, in which the failure based on the plastic strain, the stress – strain curve and the strain rate scaling effect on steel yield stress can be defined. In the present study, the steel yield strength, mass density, Young's modulus, strain rate curve and stress – strain curve are defined, which will be given below. *MAT_ELASTIC_PLASTIC_THERMAL (MAT_004) is used to model the prestress tendon. The relationship between the material properties versus temperature needs to be defined. This material model requires a range of temperature input data larger than the expected change of temperature. It is defined by *LOAD_THERMAL_LOAD_CURVE card in LS-DYNA. Besides, the LS-DYNA material model named *MAT_ELASTIC (MAT_001) is employed to model the steel pendulum impactor. The input parameters of these materials are given in Table 1.

The LS-DYNA keyword *MAT_ADD_EROSION is utilized to eliminate the damaged concrete elements which are no longer contributing to resisting the impact force. The erosion feature in LS-DYNA is important in studying the impact and blast response of RC structures, and has been commonly adopted in the previous studies [15, 16, 23, 24]. In the explicit simulation, the concrete elements will be automatically removed when the tensile stress reaches

255 the defined erosion tensile strength or the erosion principal strain. It should be mentioned that
256 if the erosion principal strain defined by users is too high, large deformation of concrete
257 elements may cause computation overflow. If this value is too low, the conservation of energy
258 and mass will not be maintained, the analysis results are therefore no longer trustworthy [23].
259 The value of 0.9 is used for the erosion criterion of concrete material in the present study after
260 trials to yield fairly good agreement with the experimental results.

261 Similarly, an effective plastic strain of steel reinforcements is defined to erode excessively
262 deformed reinforcement elements. In this study, when the plastic strain of steel material reaches
263 0.18, the element is eliminated from the analysis.

264 Table 1. Material properties of numerical model

Element	LS-DYNA model	Input parameter	Magnitude
Concrete	* Mat_072R3	Mass density	2400 kg/m^3
		Unconfined strength	34 MPa
Tendon	* Mat_Elastic_Plastic_Thermal	Mass density	7800 kg/m^3
		Young's Modulus	210 GPa
		Poisson's ratio	0.3
		Yield stress	1860 MPa
		Plastic hardening modulus	1200 MPa
		Thermal expansion coefficient	0.0001
Rebar	*Mat_Piecewise_Linear_Plasticity	Mass density	7800 kg/m^3
		Young's Modulus	210 GPa
		Poisson's ratio	0.3
		Yield stress	500 MPa
Stirrup	*Mat_Piecewise_Linear_Plasticity	Mass density	7800 kg/m^3
		Young's Modulus	210 GPa
		Poisson's ratio	0.3
		Yield stress	300 MPa
Impactor	*Mat_Elastic	Mass density	7800 kg/m^3
		Young's Modulus	210 MPa
		Poisson's ratio	0.3

265 ***2.2.3. Strain rate effect***

It is widely known that under high velocity impact or blast load, the mechanical properties of materials such as concrete and steel are different from the quasi-static conditions. Both of the compressive and tensile strength of these materials are improved under high strain rate [25-29]. The influences of strain rate on material properties and hence on the numerical simulation results have been investigated in the previous studies [15, 16, 23, 24]. Correctly modelling the strain – rate effect was found playing an important role for accurately predicting the structure responses under impact and blast loads. Usually, the strain rate effect is quantified by the ratio of dynamic-to-static strength, i.e., the dynamic increase factor (DIF) versus strain rate. A number of empirical equations have been introduced to estimate the DIF at different strain rates. It should be noted that the DIF was obtained directly from dynamic impact tests, which as commonly understood now consisted of both the material strain rate effect and lateral inertial confinement effect. Lateral inertial confinement effect is a structural effect depending on the specimen size used in the test and impact velocity, and should be removed from the testing data for deriving the true material strain rate effect [29-31]. In the present research, the DIFs of concrete compressive and tensile strength given by Hao and Hao [31] are adopted. These DIF relations eliminate the contributions of lateral inertia confinement and end friction confinement from dynamic impact tests, and therefore are more accurate in modelling the concrete material strain rate effect. The DIF relations for steel reinforcement defined by Malvar [26] are used.

The compressive DIF of concrete at the strain rate $\dot{\varepsilon}_d$ is given by the following equation:

$$CDIF = \frac{f_{cd}}{f_{cs}} = \begin{cases} 0.0419(\log \dot{\varepsilon}_d) + 1.2165 & for\left(\dot{\varepsilon}_d > 30s^{-1}\right) \\ 0.8988(\log \dot{\varepsilon}_d)^2 - 2.8255(\log \dot{\varepsilon}_d) + 3.4907 & for\left(\dot{\varepsilon}_d \le 30s^{-1}\right) \end{cases} \quad (4)$$

in which *CDIF* is the DIF for the concrete in compression; f_{cd} is the dynamic compressive strength at the stain rate $\dot{\varepsilon}_d$, and f_{cs} is the static compressive strength.

The DIF of concrete tensile strength is

$$TDIF = \frac{f_{td}}{f_{ts}} = \begin{cases} 0.26(\log \dot{\varepsilon}_d) + 2.06 & for\left(\dot{\varepsilon}_d \le 1s^{-1}\right) \\ 2(\log \dot{\varepsilon}_d) + 2.06 & for\left(1s^{-1} < \dot{\varepsilon} \le 2s^{-1}\right) \\ 1.44331(\log \dot{\varepsilon}_d) + 2.2276 & for\left(2s^{-1} < \dot{\varepsilon}_d \le 150s^{-1}\right) \end{cases} \quad (5)$$

where *TDIF* is the DIF for the concrete in tension; f_{td} is the dynamic tensile strength at the strain rate $\dot{\varepsilon}_d$, and f_{ts} is the static tensile strength.

The relationship between the tensile and compressive DIF of steel and strain rate is defined by the following equation:

$$DIF = \left(\frac{\dot{\varepsilon}}{10^{-4}}\right)^{\alpha} \quad (6a)$$

$$\alpha = 0.074 - \frac{0.04 f_y}{414} \quad (6b)$$

where f_y is the yield strength of steel in MPa. It should be noted that in this study DIF is held as constant when the strain rate is higher than 160 s^{-1} to prevent overestimation of the DIF of steel material at very high strain rate.

2.2.4. Contact definition

The commercial software LS-DYNA has introduced some contact algorithms for users to simulate the contact among the parts of numerical model such as kinematic constraint method and the penalty method [13]. Among these contact algorithms, the penalty method employed via the contact keyword namely AUTOMATIC_SURFACE_TO_SURFACE (ASTS) becomes popular and it has proven yielding reliable results [32, 33]. However, this method is complicated in term of evaluating the contact stiffness which is based on bulk modulus, the area of the

306 contact zone, the volume of the contact elements, the penalty scale factor and the scale factor
307 [13]. LS-DYNA normally suggests the default value for penalty scale factor of 0.1 and the scale
308 factor 1.0. Nevertheless, if the stiffness of the two parts in the contact is significantly different,
309 the stiffness of the softer part is taken as the contact stiffness as the default choice. The default
310 may not yield reliable results due to an excessively small stiffness. The scale factor can be,
311 therefore, manually defined by users to modify the stiffness of two parts to make them
312 compatible. The scale factor and friction coefficient of the contact algorithm used in this study
313 are given in Table 2. Besides, perfect bond between reinforcing steel reinforcement, stirrups,
314 and surrounding concrete is assumed in this study.

315 Table 2. Contact parameters

Contact components	Keyword	Input parameter	Magnitude
Concrete segments	ASTS	Static coefficient of friction	0.60
		Scale factor of slave penalty stiffness	0.10
		Scale factor of master penalty stiffness	0.10
Tendon and concrete segments	ASTS	Static coefficient of friction	0.00
		Scale factor of slave penalty stiffness	1.00
		Scale factor of master penalty stiffness	1.00

316 ***2.2.5. Finite Element Analysis Model***

317 A 3D non-linear finite element (FE) model of the scaled PCSC under pendulum impact test
318 described in Section 2.1 is created in LS-DYNA, as illustrated in Fig. 5. Both the concrete
319 column and pendulum impactor are represented by hexahedral elements with one integration
320 point. 3-nodes beam element with 2x2 Gauss quadrature integration is employed to model the
321 longitudinal reinforcing steel bars and stirrups. A convergence test is also carried out to
322 determine the optimal element size. The results indicate that the simulation converged when
323 the mesh size of concrete element and reinforcement steel is 5 mm. Further decrease in the
324 element size only has a slight variation of the numerical results but requires much longer
325 computing time and may lead to computer memory overflow. The concrete segments,

326 reinforcing steel bars and stirrups, therefore, have the mesh size of 5mm. The maximum mesh
327 size for the impactor and top concrete block is 50 mm. In this study, the 3D FE model has
328 126,407 elements consisting of 124,247 solid elements and 2,160 beam elements. To prevent
329 the initial penetration between pendulum impactor and concrete segments, the initial distance
330 between these parts is assigned to be 2.5 mm.
331 According to the material properties of tendon element introduced in Section 2.2, the pre-
332 stressing force of 30 kN was applied in the test, which is modelled here with a temperature drop
333 of 29.4^{o}C with respect to the reference temperature of 0^{o}C. The temperature of the tendon then
334 remains unchanged throughout the explicit simulation phase of the response of column
335 subjected to impact forces (see Fig.3).
336 In the experimental tests, the column foundation was anchored to laboratory floor through four
337 bolts. No vertical and horizontal displacement or rotation at the base was recorded during the
338 test [4]. To represent the actual boundary condition, all of the nodes on the bottom face of the
339 footing are constrained in all directions in the numerical model.

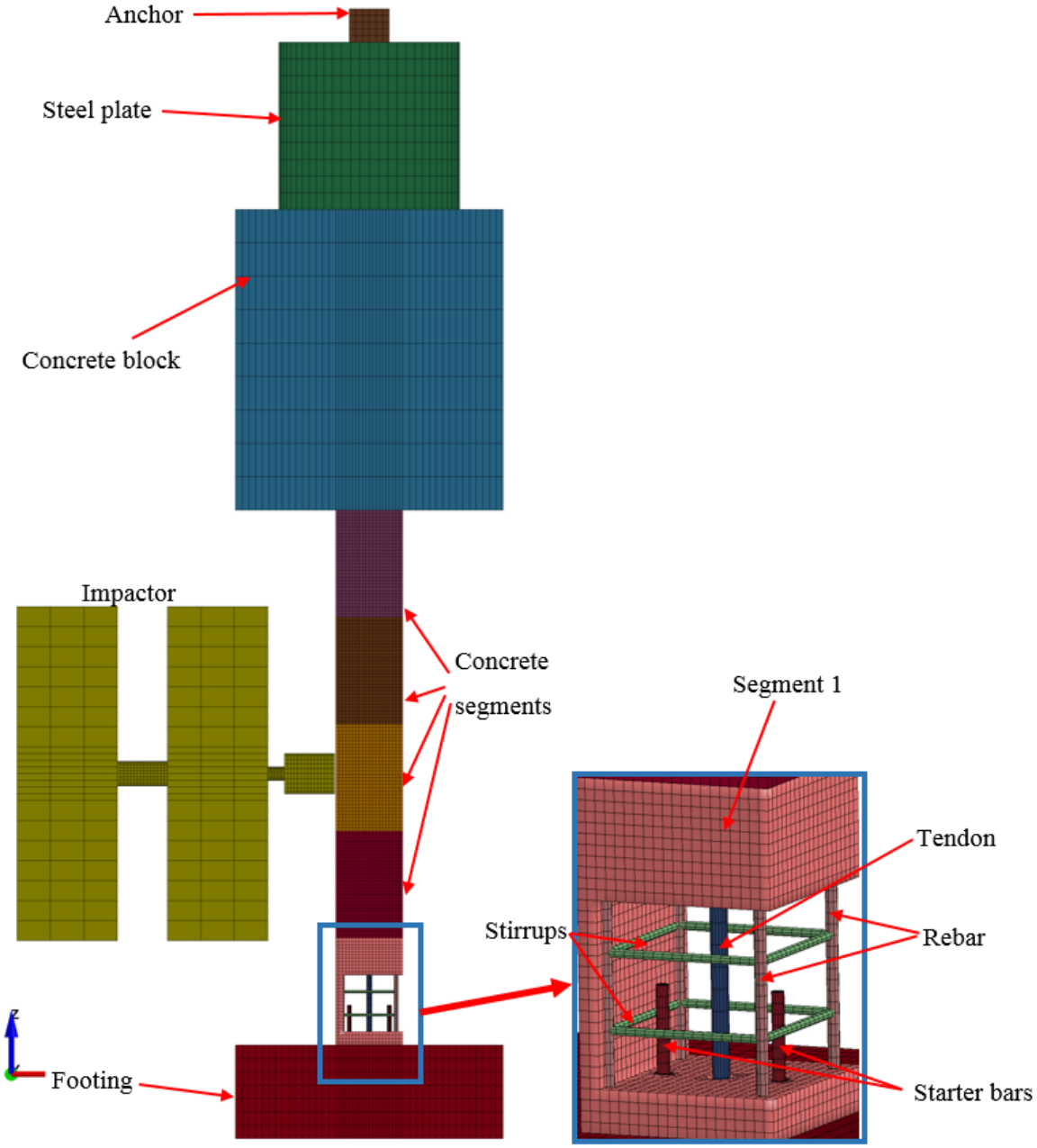

340

341 Fig. 5. Numerical model of the PCSC with pendulum impactor

342 ***2.3. Model calibration and comparisons***

343 To validate the accuracy of the FE model in predicting the column responses to pendulum
344 impact, the time histories of resultant impact force in the contact area, displacement at the center
345 of the column and damage to the column by pendulum impact are compared in this section.

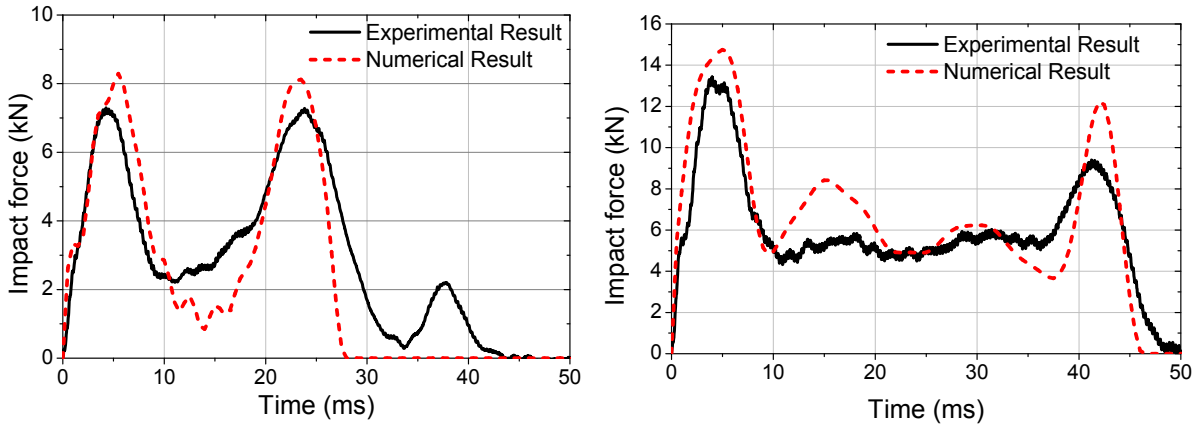

(a) Impact 1 – V = 0.23 m/s (b) Impact 2 – V = 0.64 m/s

Fig. 6. Model verification – simulation and experiment: Impact force time histories

In the first impact test, the velocity of the pendulum impactor at the time in contact with column was 0.23 m/s (Impact 1). The comparison of impact force time histories between numerical simulation and experimental test is shown in Fig. 6a. It can be seen from the figure that the numerical results agree reasonably well with the experimental test. The peak impact force and its duration in FE model are 8.29 kN and 28 ms compared to 7.30 kN and 40 ms in the experimental test, respectively. The corresponding impulse from the FE simulation and experimental tests are 117 Ns and 141 Ns, respectively. The relatively large difference between the loading duration from the FE simulation and experimental test is because only two peaks are simulated while three peaks were recorded in the test. The third peak recorded in the test was caused by a repeated impact from the impactor, i.e., the pendulum rebounded and impacted on the column again. Although the third impact force is relatively small, it led to a larger column response as shown in Fig. 7. To prevent this repeated impact, in the subsequent tests, a steel beam was used, which was quickly inserted into the steel frame when pendulum rebounded to stop it impacting the column specimen again. When the release angle was 7 degrees the impact velocity was 0.64 m/s (Impact 2), the impact force time history predicted by the FE model again compares well with the experimental result as shown in Fig 6b. The peak impact force, duration and impulse in the numerical model are 14.76 kN, 46 ms and 327.6 Ns while those in

366 experimental test are 13.44 kN, 48 ms and 300 Ns, respectively. Fig. 7 compares the numerical
367 simulated and recorded displacement time histories at the center of column. As shown although
368 the difference in the maximum displacement from Impact 1 is observed because of the repeated
369 impact as explained above, the global trend of two curves is in good agreement. Comparison of
370 the displacement time histories of Impact 2 shows better agreement because the repeated impact
371 as discussed above was prevented in the test. The maximum displacement obtained from
372 numerical simulation agrees well with the recorded maximum displacement. Because the
373 impact forces in these two tests are relatively small, no concrete damage is observed in both the
374 experimental test and numerical simulation.

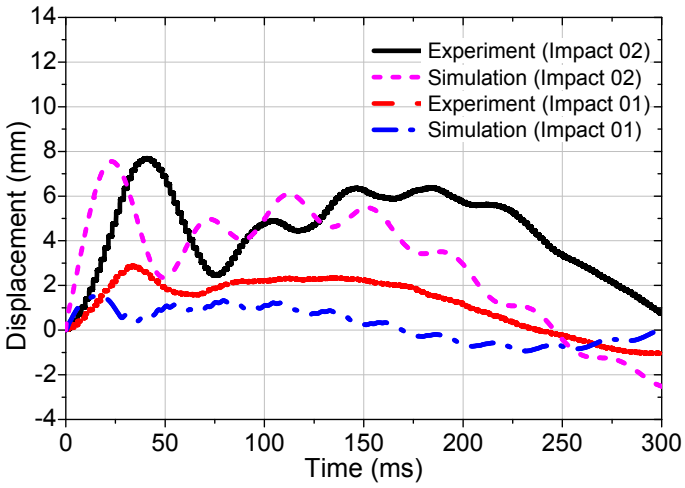

375

376 Fig. 7. Model verification – Displacement at the center of the column

377 When the impactor was released at 15 degrees in Impact 3, the impact velocity was 1.37 m/s,
378 the FE analysis results and testing results are compared in Fig. 8. It is very clear from Fig.8a
379 that after the first peak impact force occurred owing to the interaction between the impactor
380 and the column, another four peak impact forces were recorded in both numerical simulation
381 and experimental test with the same period (about 20 ms). This observation can be attributed to
382 the high-frequency concrete segment vibration. As shown in Fig.9, while the top of the column
383 vibrates around its original position, the response of the five concrete segments consists of the
384 segment-self vibration and the column vibration. The natural frequency of the concrete segment

385 is considerably higher than that of the column with five segments. For example, the vibration
386 period of a single segment was 40 ms while that of the column was more than 200 ms from the
387 displacement response time history shown in Fig. 9a. It should be noted that the vibration period
388 of concrete segment will be reduced when the impact energy increases because of the change
389 of boundary condition caused by relative slippage between segments. When the impact velocity
390 was 1.37 m/s, the slippage between the concrete segments occurred and it affected the stiffness
391 of the concrete segments. As a result, during Impact 3, the vibration period of the segment is
392 reduced to around 20 ms (see Fig. 9b). This vibration of the concrete segment in contact with
393 the impactor resulted in the four peaks in the impact force time history at 20ms, 42ms, 63ms,
394 and 83ms shown in Fig. 8a. During the impact event the impact force will increase if the
395 impactor and the impacted segment tend to move towards each other and it will decrease if the
396 two parts tend to move together in the same direction. Further investigation in Fig. 9b shows
397 that the segment-self vibration has a period approximately of 20 ms which matches well with
398 the period between the peaks in Fig. 8a. It is noted that the instants of peak impact force shown
399 in Fig. 8a and the peak displacement shown in Fig. 9b coincide with each other.

400 The peak impact force and impact duration in FE model are 20.70 kN and 93 ms, which
401 compared well to 20.91 kN and 93 ms in the experimental test (see Fig.8a). The impulse
402 predicted from the numerical model is 537.4 Ns which is just 3.7% less than that of the
403 experimental test (about 557.8 Ns).

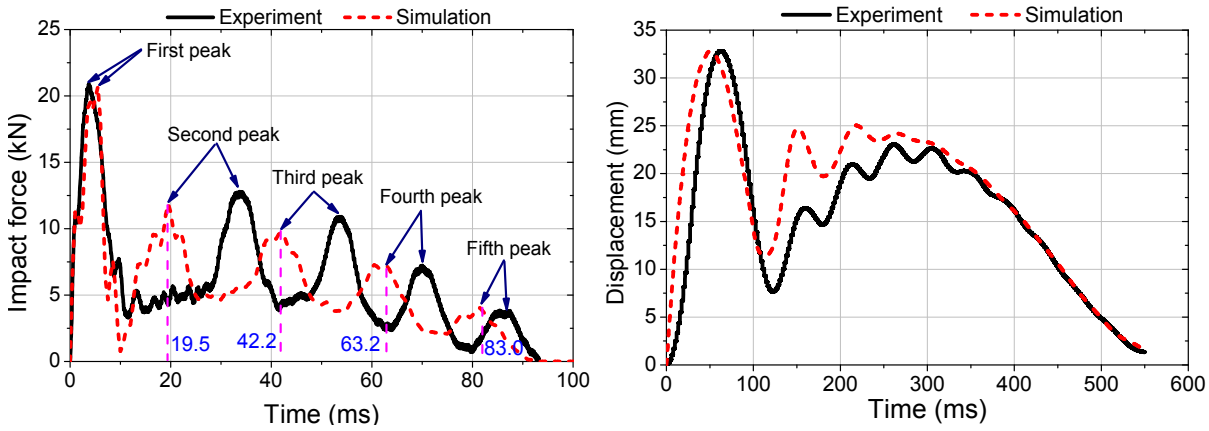

(a) Impact force time history (b) Displacement at the center of column

Fig. 8. Model verification – simulation and experiment: Impact 3

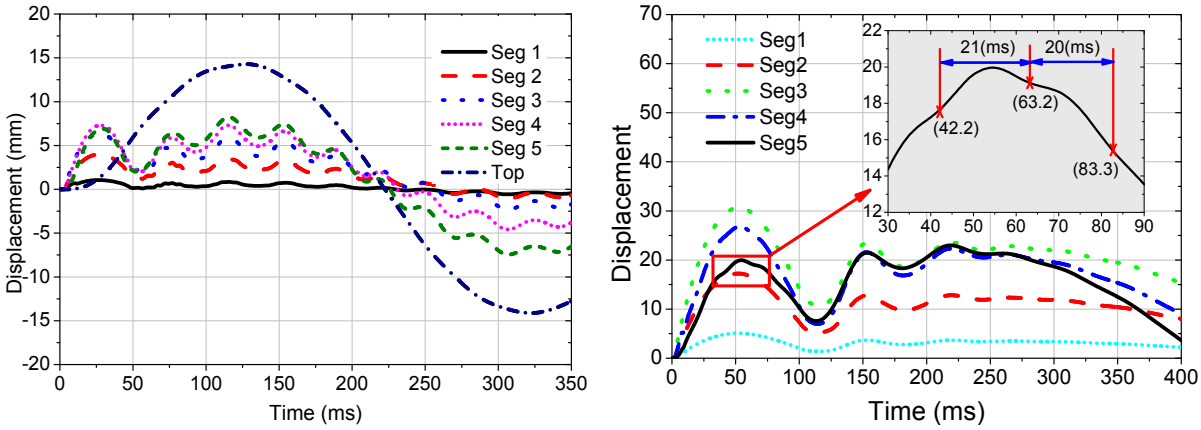

(a) Impact 02 (b) Impact 03

Fig. 9. Displacement time histories by numerical simulation

In terms of the displacement time history at the center of column, the maximum values from the two models agree very well with 32.75 mm from the numerical simulation and 32.80 mm from the experimental test (see Fig. 8b). Although, a faster displacement response can be found in the numerical model compared to experimental test (about 18ms) due to a faster peak impact force, the global trends of the displacement response histories from numerical simulation and experimental test are in good agreement. Fig.10 shows the comparison of numerical and experimental column deformation and damage corresponding to the impact velocity of 1.37 m/s at different time instants. As shown the damage at the top left corner of Segment 3, the relative

418 shear slip and joint opening between Segments 3 and 4, and the joint opening at the base are
419 well simulated in the numerical model.

420 The above observations and comparisons indicate that the numerical model reliably predicts
421 impact response of the PCSC. The current FE model also has the ability to capture the opening
422 between segments, shear slip, local damage, plastic deformation and failure modes of the
423 column.

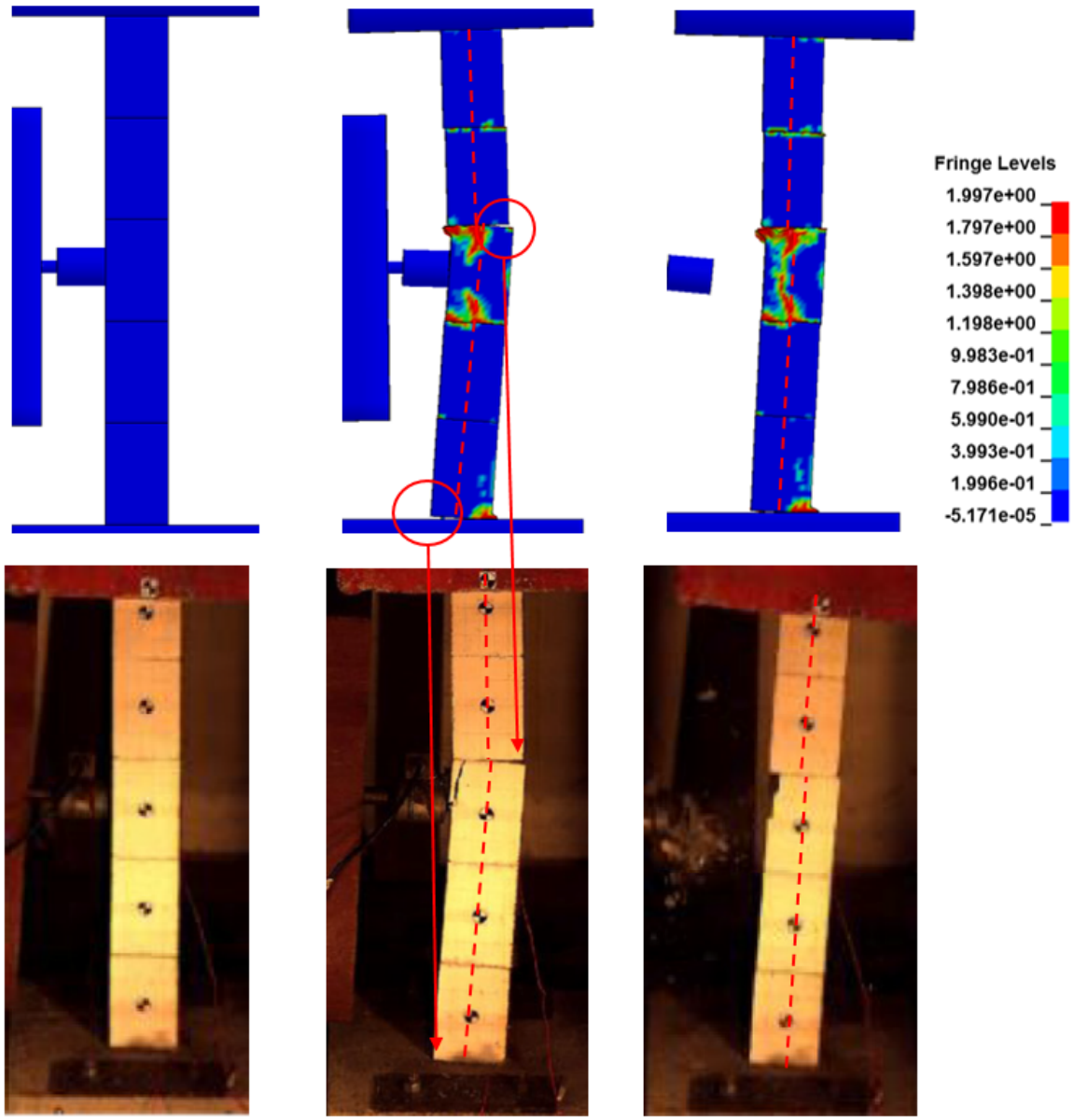

424

425 Fig. 10. Progressive damage of the column under Impact 3

3. Numerical results and parametric study

Using the same material models, strain rate relations of concrete and steel, prestressing method, and contact definitions, the above calibrated model is extended to create a full-scale model of a PCSC. The configuration of the column is presented in Fig. 11. The dimensions of the column are 600 mm in depth, 600 mm in width, and 4800 mm in height. The top concrete block and steel plates in the test are replaced by a console beam placed on the top of the column. The size of the footing used in this model is 2600 mm x 2600 mm x 1000 mm. The design dead load is equal to 10% of the axial compressive capacity of the column ($0.1f'_cA_g$), where f'_c is the concrete compressive strength, and A_g is the gross cross-section area of the column. Four post-tensioned tendons (25 mm in diameter) are employed in the full-scale model and placed at the four corners of the column. The total area of four tendons is 1974 mm^2 with the initial prestress load equal to $0.36f_u$, where f_u is the tensile strength of the tendons. It is equal to $0.11f'_cA_g$. The hole left for the tendon is 35 mm in diameter. The compressive strength of concrete as well as the tensile strength of the tendon and reinforcing steel bars are the same as those previously presented. According to the convergence test, the smallest mesh size of the solid elements used in the model is 20 mm. The maximum mesh size for the top concrete beam is 100 mm. In this study, the 3D segmental bridge column model has 301,978 elements consisting of 290,036 solid elements and 11,942 beam elements.

The solid steel impactor is replaced by a 3D vehicle model with 216,400 elements and 220,499 nodes, representing the 1129 kg 1998 Chevrolet S10 pickup (Fig. 12). This vehicle model was downloaded from National Highway Traffic Safety Administration (NHTSA) [34]. The accuracy of the vehicle model has been validated by FHWA/NHTS National Crash Analysis Center at the George Washington University. According to the AASHTO-LRFD [35], the impact point locates at 1.5 m above the top of the footing in the simulation (Fig. 11).

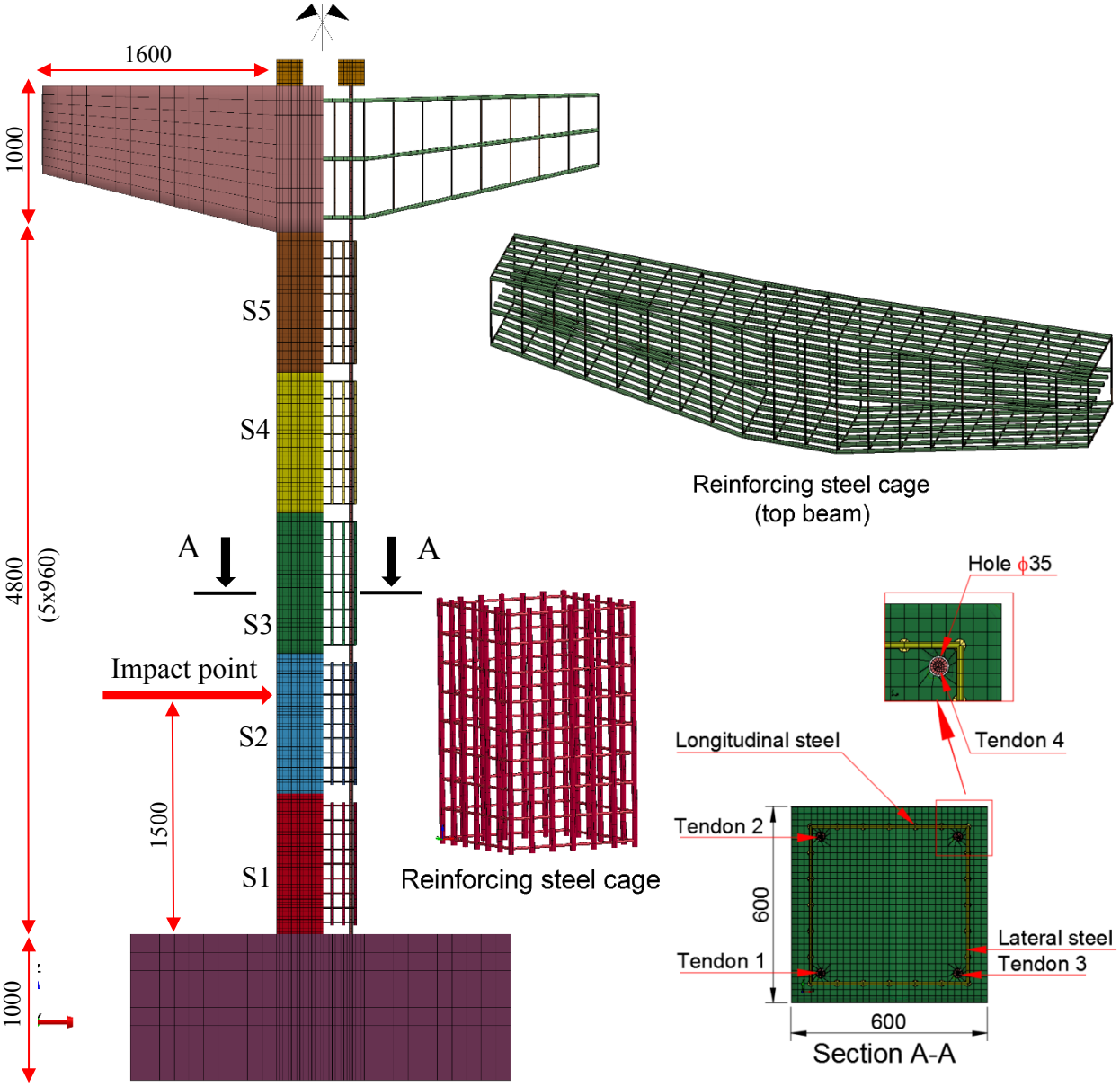

Fig. 11. The configuration of the PCSC (reference case – C0)

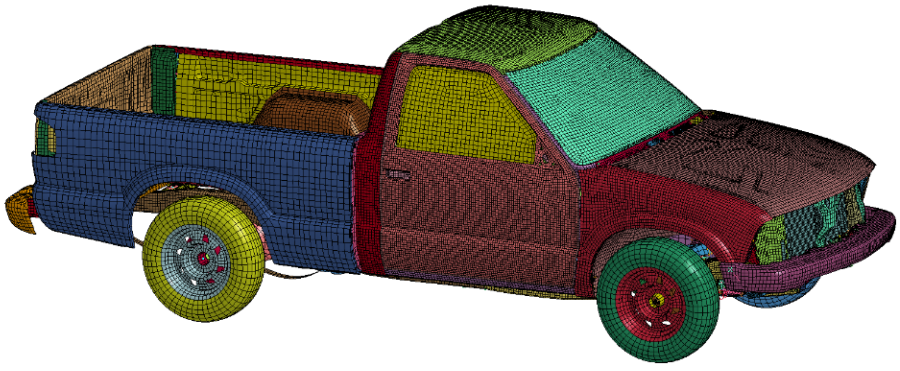

Fig. 12. 1998 Chevrolet S10 pickup FE model

Under the impact of a Chevrolet S10 pickup at the velocity of 70 km/h, the calculated impact force time history on the PCSC is presented in Fig. 13a. As shown, after gradually increasing to around 300 kN, the vehicle's engine collides with the column at t = 30 ms (see Fig. 13b and Fig. 13c) and it generates the peak impact force of 1861.5 kN (t = 35.5 ms). The impact force then significantly decreases to about 250 kN at t = 40 ms before reducing to zero at t = 160 ms. The impulse of the impact force is 22.96 kN.s.

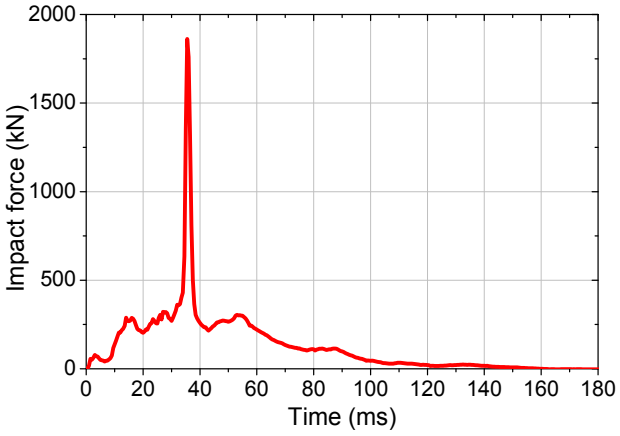

(a) Time history of the impact force

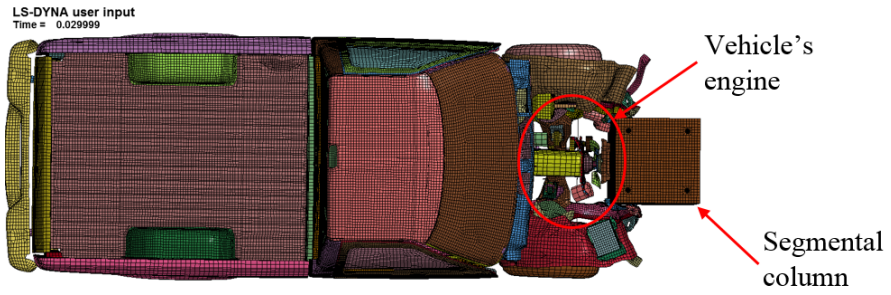

(b) Vehicle's engine starts to collide the column (t = 30 ms)

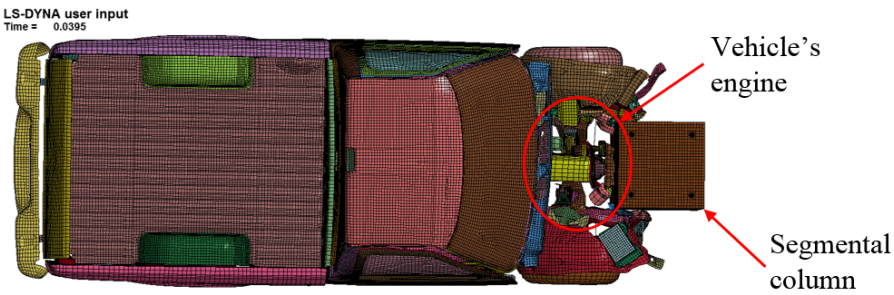

(c) After vehicle's engine hits the column (t = 39.5 ms)

Fig. 13. Vehicle collision between the PCSC and Chevrolet S10 pickup

467 The progressive deformation, displacement and damage to the PCSC and the vehicle are shown
468 in Fig. 14. After the impact force has reached the peak, the relative lateral shear slips between
469 the impacted segment and its adjacent segments are observed. As shown in Fig. 14b, at t = 40
470 ms the relative lateral displacement between Segment 2 (impacted segment – S2) and S1,
471 between S2 and S3 are 17.7 mm and 6.4 mm, respectively. The slip between S1 and footing is
472 5mm. The relative displacements between the other segments are also observed, as illustrated
473 in Fig. 14b. It could be explained that under high rate impulse load, the local response or shear
474 deformation governs the behavior of the PCSC while the friction force between the segments
475 resulted from the initial pre-stressing load and the self-weight of the column is insufficient to
476 resist the shear force. It leads to the lateral shear slips between the segments in the PCSC.
477 Moreover, the relative displacement between the impacted segment and its adjacent segments
478 is larger than the other segmental joints. The column then continues deforming to reach the
479 maximum positive displacement at t = 221 ms and the maximum negative displacement at t =
480 491 ms. As can be seen in Fig. 14c, when the base stops moving at the residual displacement
481 of 9 mm, the other parts of column continues vibrating freely around the residual displacement
482 of 25 mm. The 25 mm diameter tendon is placed inside the 35 mm posttensioning duct of the
483 segments. There is, in general, a nominal gap of 5 mm between tendons and each side of the
484 concrete segments. The total gap between tendon and concrete segment is 10 mm. Therefore
485 after suddenly sliding 5 mm at 50 ms due to the impact force, the bottommost segment is in
486 contact with the post-tensioned tendon. Both the concrete segment and tendon then slide with
487 a continuous motion to the maximum value of 9 mm. For Segment 2, the contact force between
488 concrete segments and the tendon is insufficient to resist the huge direct shear force from the
489 vehicle collision. Hence, before ceasing the sliding of Segment 2 at 17.7 mm (35 ms), concrete
490 damage is found in the duct of the segment. The relative displacement of Segment 2 with respect
491 to the footing is about 27 mm. After the loading phase (160 ms), the contact force from the

tendon is inadequate to pull the segments back to the original position and thus the relative lateral displacement between the concrete segments is nearly unchanged (see Fig. 14b). The column, as well as the concrete segments then vibrates freely around their residual position. With the effect of the large inertial resistance force and located at a distance from the impact point, the column top responds slower than the other parts in the first stage of impact event (see Figs. 14b and 14c).

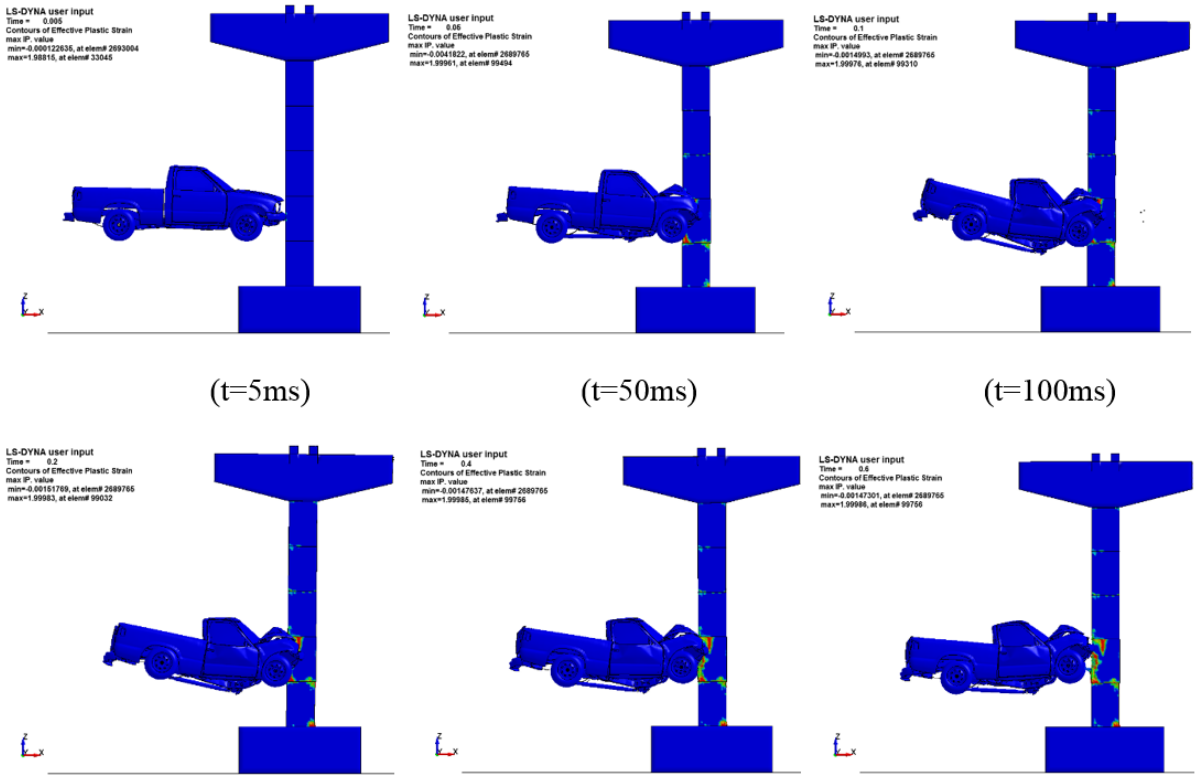

(t=5ms) (t=50ms) (t=100ms)

(t=200ms) (t=400ms) (t=600ms)

(a) Progressive collision between Chevrolet S10 pickup and the PCSC

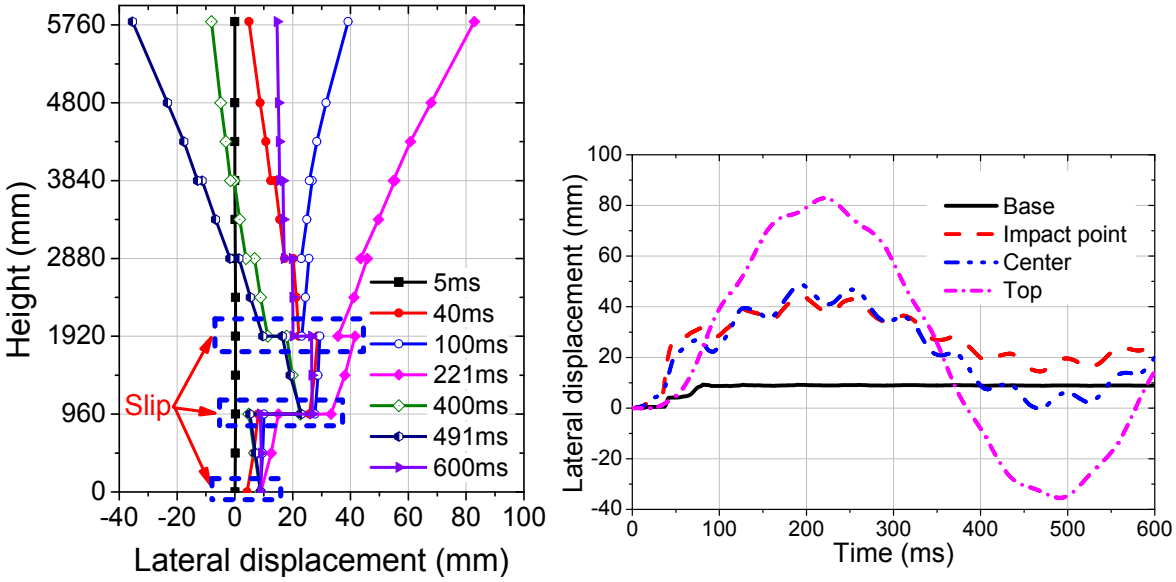

(b) Column displacement (c) Time histories of displacement

Fig. 14. Response of the PCSC under 70 km/h vehicle collision

The pre-stressing force histories of the four tendons are shown in Fig. 15. The prestress level in the tendons nearly remains stable (335.6 kN) before the vehicle's engine impacts to the column. After that, due to the huge impact force from the collision, the opening at the second joint and the large shear slips between the segments appear. The prestress forces slightly increase in the two tendons on the tension-side (Tendons 3 and 4) and and those in the compression side (Tendons 1 and 2) decrease. The prestress force then vibrates around its initial stress level with a minor prestressing loss (1%) being recorded. At the time the column top reaches the maximum lateral displacement, the prestress force reaches the highest value of 382.2kN, about 14% higher than the initial stress level. It is worth mentioning that these changes in the tendon stresses cannot be monitored if the other methods reviewed above are used to model the pre-stressing of concrete structures.

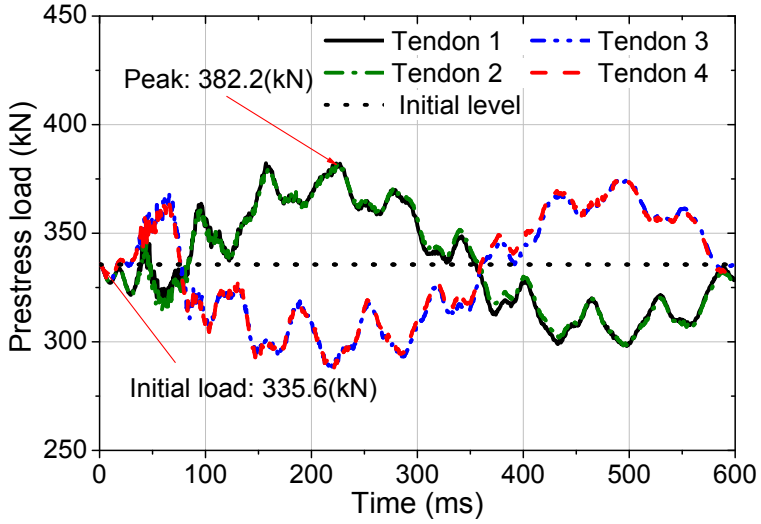

514

515 Fig. 15. The prestress load time history in four tendons

516 To further investigate the impact response of the PCSCs, a series of simulations are carried out
517 to study the effect of the vehicle energy and column parameters on the column responses. These
518 include the initial pretress level, number of segments, reinforcing steel ratio, and impact energy.

519 ***3.1. Effect of initial pre-stressing level***

520 The behavior of PCSCs under vehicle collision with different initial prestress levels including
521 $0.089f'_cA_g$ (PL30), $0.11f'_cA_g$ (C0 and PL60_2), $0.15f'_cA_g$ (PL50), and $0.2f'_cA_g$ (PL60_1) is
522 studied in this section. The description of these cases is given in Table 3. The initial compressive
523 stress on concrete is varied from 9% to 18% of the column's capacity as indicated in Table 3.

524 Table 3: Input parameters of the PCSCs with different initial pre-stressing loads

Column	Tendon			Initial prestressing load			
	Diameter	Area	Total areas	$\%f_u$	Load	Total load	$\%f_cA_g$
	mm	mm^2	mm^2		kN	kN	
C0	**25**	**490.9**	**1963.5**	**36.6**	**334.2**	**1336.7**	**10.9**
PL30	25	490.9	1963.5	30.0	273.9	1095.6	9.0
PL50	25	490.9	1963.5	50.0	456.5	1826.1	14.9
PL60_1	25	490.9	1963.5	61.2	558.8	2235.1	18.3
PL60_2	**20**	314.2	1256.6	61.6	360.0	1440.0	**11.7**

As presented in Fig. 16a, the impact force time histories of these columns show very small differences. The peak impact force of Column PL30 is 1842.6 kN, which is just about 1.5% and 1.8% smaller than that of Column PL60_1 (1860.4 kN) and Column PL60_2 (1877.5 kN), respectively. The impact duration of Column PL30 (167 ms) is slightly longer than that of Column PL60_1 (150 ms). Similar impulses are also recorded in the five columns (approximately 23.0 kNs). This observation can be explained that under impact conditions, the impact force and impulse depend primarily on the initial impact energy and the concrete column – impactor interaction [21], which depends on the local stiffness at the beginning stage of the impact event [36]. The change of the initial stress level enhances the strength and initial stiffness of PCSCs [11], i.e., the global stiffness of the column, but has no effect on the local contact stiffness. As a result, the increase of prestress level does not have noticeable influences on the impact force of the PCSCs. The numerical results of these columns are presented in Table 4.

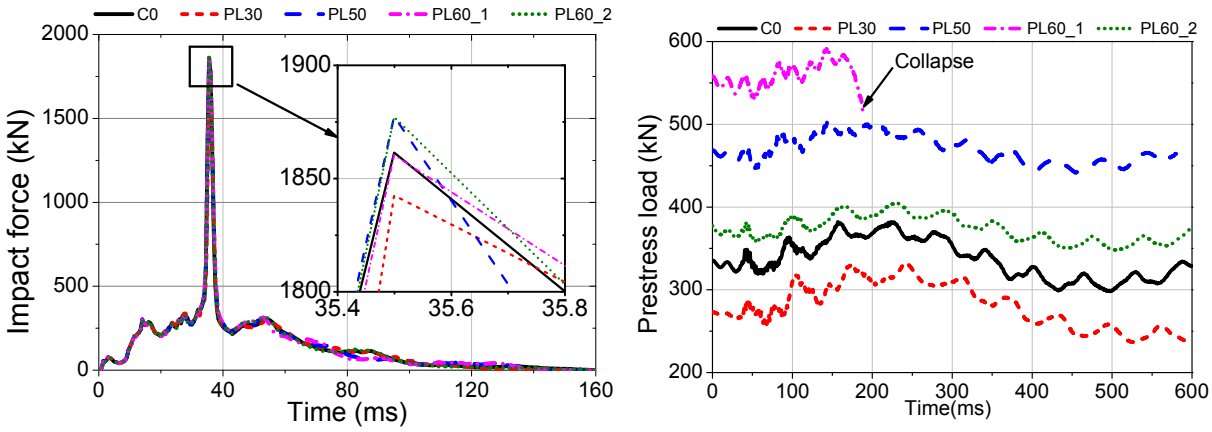

(a) Impact force – time histories (b) Prestress load – time histories

Fig. 16. The time histories of the impact force and prestress force corresponding to the different initial prestress levels

Conversely, the initial prestress level is significantly important to the deformation of the PCSCs. Higher initial axial stress on the concrete column leads to enhancement of the friction

543 force between the concrete segments and thus improves the shear strength of the column. As a
544 result, the relative lateral displacement between the segments is reduced. As can be seen in
545 Fig.17, the relative shear slip at the base is about 13 mm, and that between the impact point of
546 Column PL30 and the footing is around 37 mm. The corresponding results of Column PL50 are
547 only 6 mm and 20 mm, respectively. Besides, the column with higher initial prestress force
548 leads to smaller lateral displacement than the counterparts (see Fig.17). However, when the
549 initial axial load on concrete increases to 0.183 $f_c^{'}A_g$ (PL60_1), due to high compression stress
550 from the initial axial load and the collision, severe concrete damage at the base of column is
551 found at 180 ms and leads to the column collapse. These results demonstrate that a balance of
552 the prestress force level needs be carefully determined. A larger prestress level is generally
553 desirable provided it does not cause premature failure of the column when acted together with
554 the impact load.

555 Interestingly, with different pretressing levels in the tendons but similar axial compression load
556 on concrete, Columns C0 and PL60_2 show the same response to vehicle collision (Fig.17).
557 The detailed comparisons are presented in Table 4. This is because the tendons are still in its
558 elastic range at these different prestressing levels.

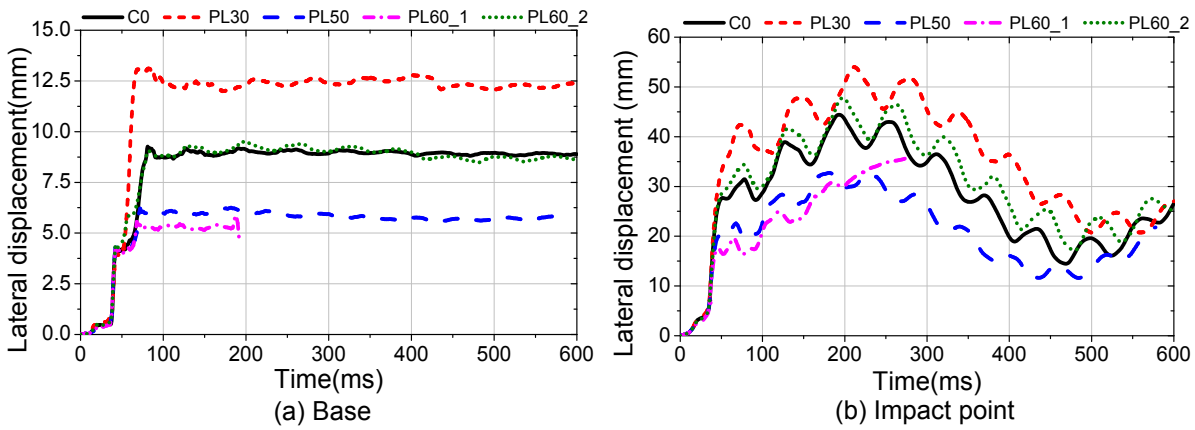

559

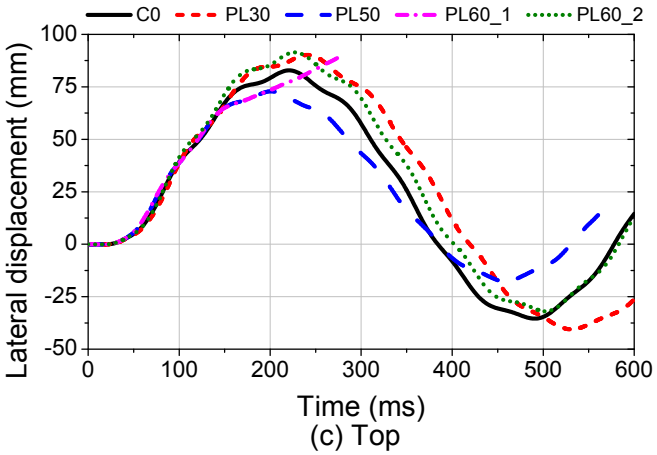

560

561 Fig. 17. Displacement time histories of the column with varied initial prestress levels

562 Table 4. Comparisons of the column responses with different initial prestress levels

Parameter			PL30	C0	PL50	PL60_1	PL60_2
Impact force	Peak	kN	1842.6	1861.5	1877.4	1860.4	1877.2
	Duration	ms	167.0	160.0	147.0	150.0	159.5
	Impulse	kNs	22.8	23.0	22.9	23.0	22.8
Shear slips	Joint 1	mm	9.6	8.9	6.3	--	8.9
	Joint 2	mm	23.8	17.0	11.4	--	18.0
	Joint 3	mm	13.2	6.6	4.6	--	6.1
Maximum displacement	Top (positive)	mm	90.2	82.8	72.9	--	91.5
	Top (negative)	mm	-40.5	-35.4	-17.7	--	-33.0
	Center	mm	54.0	44.4	32.7	--	46.0
Peak prestress load		kN	332.0	382.2	504.9	--	405 .0

563 -- Column collapsed

564 Fig. 16b shows the prestressing force time histories in the tendons. With larger lateral
565 displacement, the increase of prestressing force in the tendon of Column PL30 is, therefore,
566 higher than the other columns. The peak prestressing force in the tendon of Column PL30 (332
567 kN) is about 22% higher than the initial prestress load (273.9 kN). That result reduces to 12%
568 in Column C0, 8% in Column PL50, and 6% in Column PL60_2. Because of the damage and
569 failure of Column PL60_1 at t = 180ms, the prestress load in the tendon then plummets.

570 ***3.2. Effect of number of segments***

In this section, numerical simulations are conducted to study the effect of number of segments on the responses of PCSCs under vehicle collision. Four segmental columns of the same height, but with different number of segments are employed in the analysis. They are designated as NOS2 (2 segments), NOS4 (4 segments), C0 (5 segments), and NOS8 (8 segments). The same 1998 Chevrolet s10 pickup with velocity of 70 km/h is considered in the analysis. As shown in Fig. 18, although the column with more segments has smaller peak impact force and longer impact duration because it is more flexible, the differences in the impact force are marginal and the impulses are almost identical (see Table 5). This is because, as discussed in the previous section, the impact force highly depends on the contact stiffness between the impactor and the concrete segment. Changing the number of segments mainly changes the global stiffness of the columns [4] but does not affect the contact stiffness. Moreover, as can be seen in Fig. 19a, the column has not experienced large displacement response during the impact force phase. Therefore, the global stiffness of the column has only a minor effect on the impact force between vehicle and column. As a result, the effect of the number of segment on the impact force is insignificant.

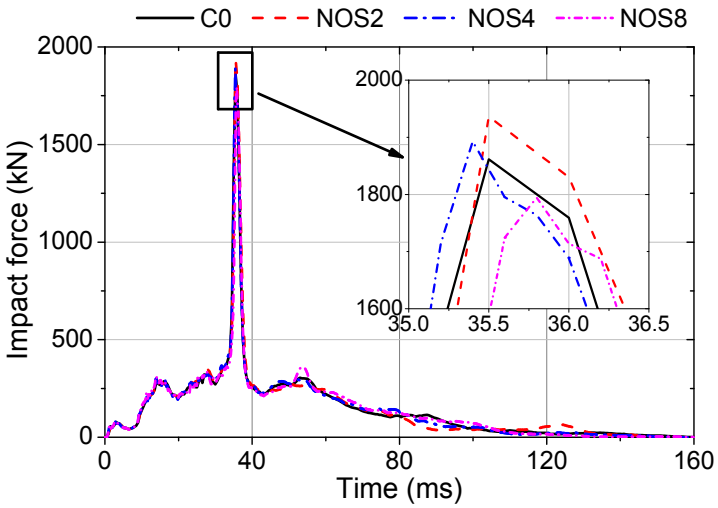

Fig. 18. Impact force time histories with varied number of segments

On the other hand, the lateral and residual displacements of the PCSC have a close relation with the number of concrete segments. Due to the relatively smaller stiffness, the PCSC with more segment joints experiences higher lateral displacement at the column top. Moreover, under lateral impact force, the column with more concrete segments shows more joint shear slips. Thus, the self-centering capacity of segmental column increases when the number of segments decreases (see Fig. 19b and Table 5). The same observation was presented in the experimental tests [4]. As shown in Fig. 19, the maximum lateral displacement of Column NOS8 (90.3 mm) is nearly 1.7 times larger than that of Column NOS2 (53.0 mm). Besides, the residual displacement of Column NOS8 is about 40 mm while those of Columns C0, NOS4, and NOS2 are 27 mm, 26 mm, and 6.0 mm, respectively.

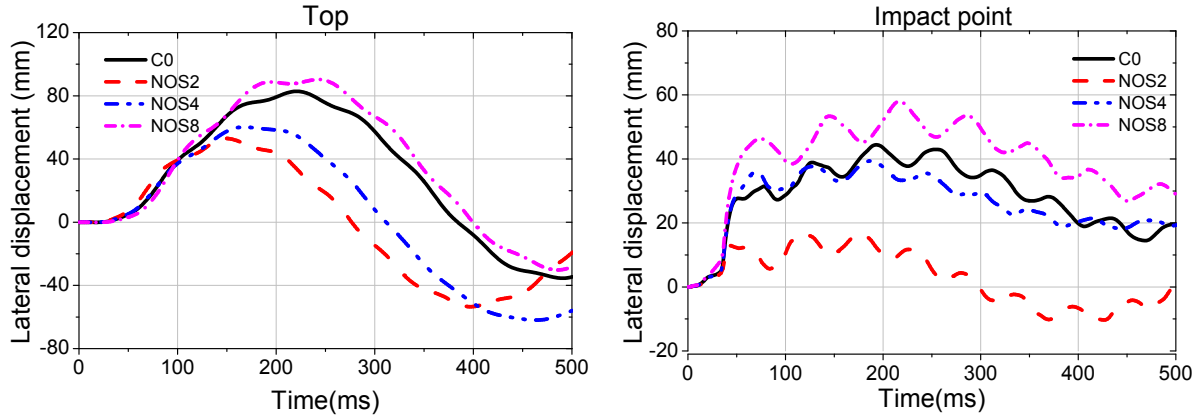

Fig. 19. Lateral displacement of PCSC with varied number of segments

The damage of the impacted concrete segments of these four columns are presented and compared in Fig. 20. The failure mode of the PCSCs is obviously affected by the number of segments. Severer damage of concrete material around the impact area is observed on the columns with more segments (Columns C0 and NOS8) while Column NOS2 exhibits more concrete cracks at the rear sides opposite the impact point. The length of concrete cracked area of Column NOS2 is approximately two times of the section depth as shown in Fig. 20. This phenomenon is very similar to the monolithic column under impact test with concrete cracks observed at the rear concrete surface at the impact point [4]. It could be explained that when

the height of concrete segment is relatively large compared to the section depth, compressive stress wave propagates from the impact point and reaches the opposite side of the impacted segment before reaching the joints as illustrated in Fig. 21. As a result, the mid-span of the segment deforms. The segment bends to cause flexural cracks on the large segment. To reduce the flexural cracks of the impacted segment, the compressive stress wave from impact event should reach the segment joints before reaching the opposite side of the concrete segment. Then slips and opening between the concrete segments might be induced to dissipate the energy and mitigate the flexural response of the segment. For this reason, the height-to-depth ratio of concrete segment, thus, should be smaller than two to inhibit an undesirable local damage at the rear concrete surface.

On the other hand, columns with more segments suffer severer local damage than those with less number of segments (see Fig. 20). This can be attributed to the strong reflected stress wave from the segment joints. These different damage mechanisms need be carefully considered when designing the segmental columns to resist impact forces.

Based on the numerical results, the crack patterns and damage of concrete under impact force are illustrated in Fig.21.

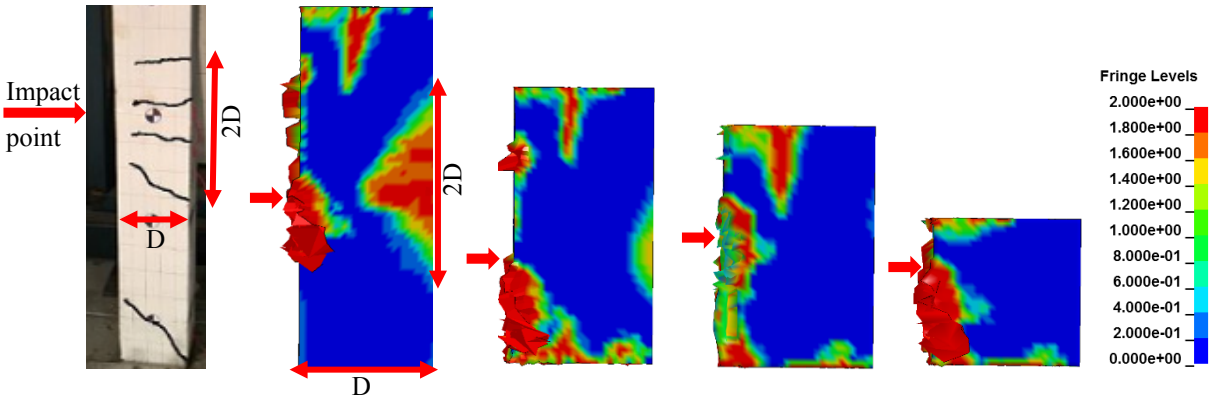

Fig. 20. Plastic strain of the impacted segment with varied number of segments

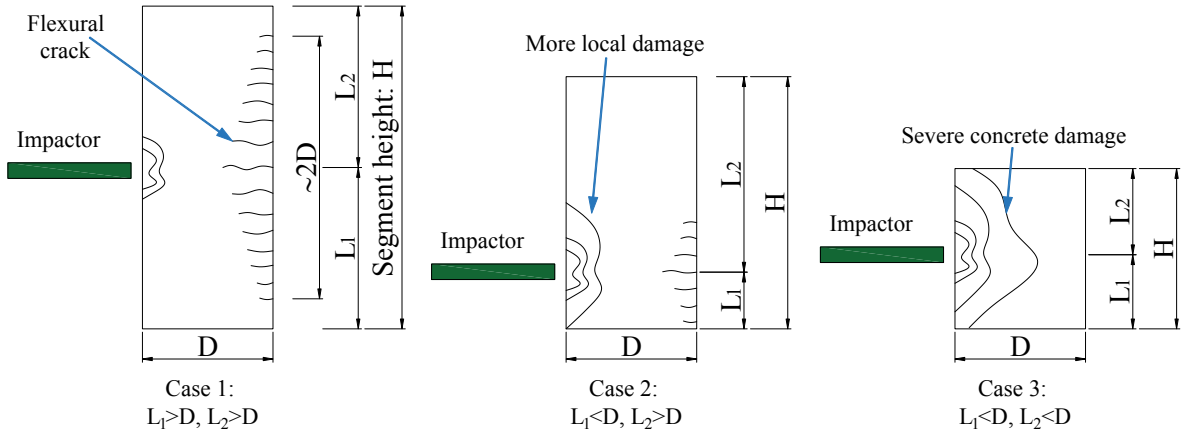

Fig. 21. The crack patterns and damage of concrete segment with different segment height

Table 5. Comparisons of the column responses with different number of segments

Parameter			NOS2	NOS4	C0	NOS8
Segment height		mm	2400	1200	960	600
Impact force	Peak	kN	19360	1893	1862	1794
	Duration	ms	150	155	160	169
	Impulse	kN.s	23.1	22.9	22.9	22.8
Maximum displacement (top)		mm	53.0	60.2	82.9	90.3
Residual displacement (impact point)		mm	6.3	26.0	27.0	40.0

3.3. Effect of concrete strength

To investigate the influences of concrete strength on the impact response of PCSCs, the compressive strength is varied from 20 MPa to 80 MPa, resulting in an increase by 2 times in the concrete modulus of elasticity. Four columns with four concrete strengths including CS20 (20 MPa), C0 (34 MPa), CS60 (60 MPa), and CS80 (80 MPa) are considered. All the other conditions including vehicle velocity remain unchanged as described above for Column C0. As shown in Fig. 22a, the impact force increases with the concrete strength but the change is minor (about 8%) with the concrete strength varying from 34 MPa to 80 MPa. Except for Column CS20, the peak impact force is 1504 kN, around 25% smaller than that of the other columns. Column CS20 exhibits severe damage on the concrete surface after the vehicle's frontal collides with the column. The stiffness of the contact area is, therefore, reduced before the vehicle's engine hits the column, which results in the significant decrease of the peak impact force

compared to the other considered columns. The damage to concrete surface of Columns C0, CS60, and CS80 is almost similar, therefore leading to the similar peak impact force and impact duration. The impulses of the impact force of these columns are almost identical (approximately 23 kNs) with the difference less than 3% (see Fig. 22a). The same observation was reported in the impact behavior of reinforced concrete beams with different concrete strengths by Pham and Hao [21]. The increase of concrete strength reduces the lateral displacement and residual displacement of PCSCs, but the change is marginal when the strength of concrete is higher than 60 MPa, shown in Fig. 22b. As previously discussed, due to the high contact force between segments and tendons, concrete damage is observed inside the concrete hole. Thus, increasing the strength of concrete material tends to reduce the concrete damage leading to diminishing the residual displacement of the PCSCs.

The concrete strength has a noticeable effect on the failure mode of PCSC as shown in Fig. 23. After reaching the maximum displacement at 260 ms, Column CS20 collapses because of severe concrete damage at the base while the PCSCs with concrete strength from 34 MPa to 80 MPa experience local concrete damage and minor damage at the base.

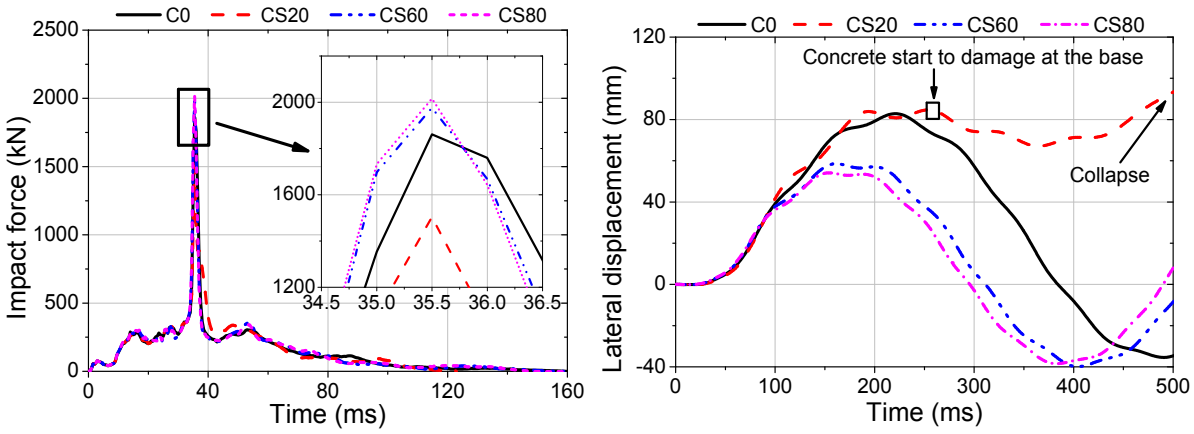

(a) Impact force time histories (b) Top displacement time histories

Fig. 22. Impact responses of PCSCs with varied concrete strength

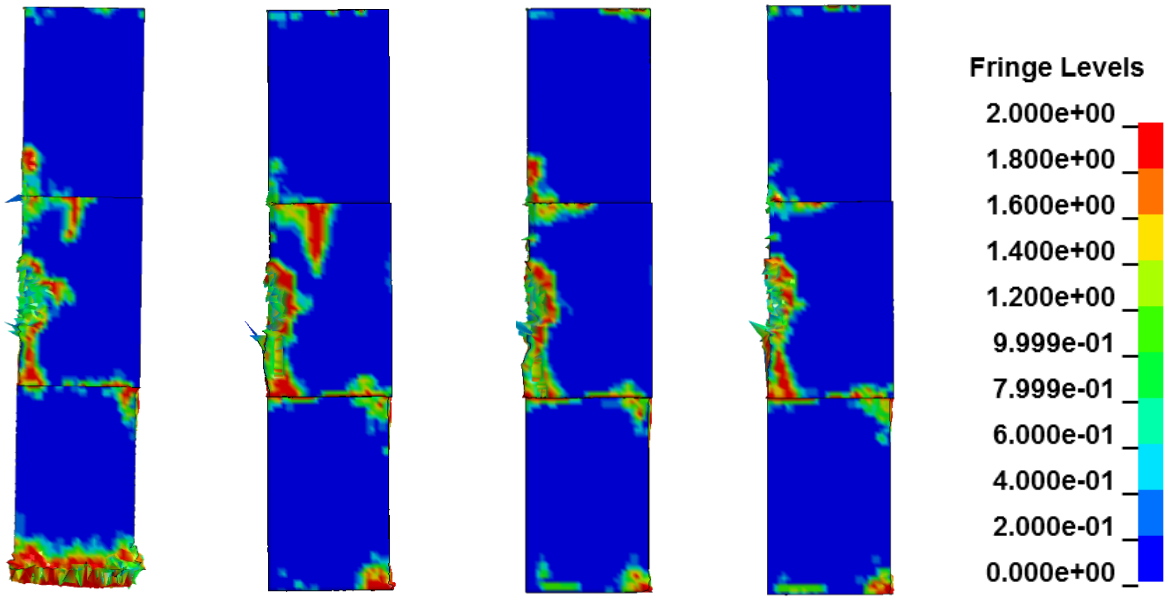

660

661 20 MPa 34 MPa 60 MPa 80 MPa

662 Fig. 23. Plastic strain of the first three segments with different concrete strength (t = 500ms)

663 ***3.4. Effect of impact energy***

664 In this section, responses of column C0 subjected to impact from the same vehicle model at
665 four different velocities, namely VL50 (50 km/h), VL60 (60 km/h), C0 (70 km/h), and VL80
666 (80 km/h), are compared to investigate the effect of impact energy on the column's
667 performance. It can be seen from Fig. 24 that the impulse increases with the impact velocity but
668 the change of the peak impact force does not follow a clear trend. The peak impact force
669 significantly increases from 314.5 kN (VL50) to 1861.5kN (C0) and the impulse rises by
670 approximately 40% from 16.58 kNs (VL50) to 22.93 kNs (C0). Interestingly, although the
671 impulse still grows to 25.94 kNs in Column VL80, the peak impact force suddenly drops to
672 1687.8 kN. This is caused by the local damage of concrete after the frontal of vehicle collides
673 on the column with a relatively high velocity. Thus, the contact stiffness between vehicle's
674 engine and concrete column reduces leading to the decrease of the peak impact force. The
675 impact force curve, therefore, shows a longer duration. This observation again proves that the
676 impact force profile is highly dependent on the concrete column – vehicle interaction. Damage

to concrete surface during the collision of the column with vehicle bumper before the collision with the solid vehicle engine significantly affects the peak force and duration of impact events. Moreover, increasing the vehicle velocity or impact energy does not always increase the peak impact force on concrete structures. Thus, to design concrete structures under vehicle collision, both peak impact force and impulse should be taken into account.

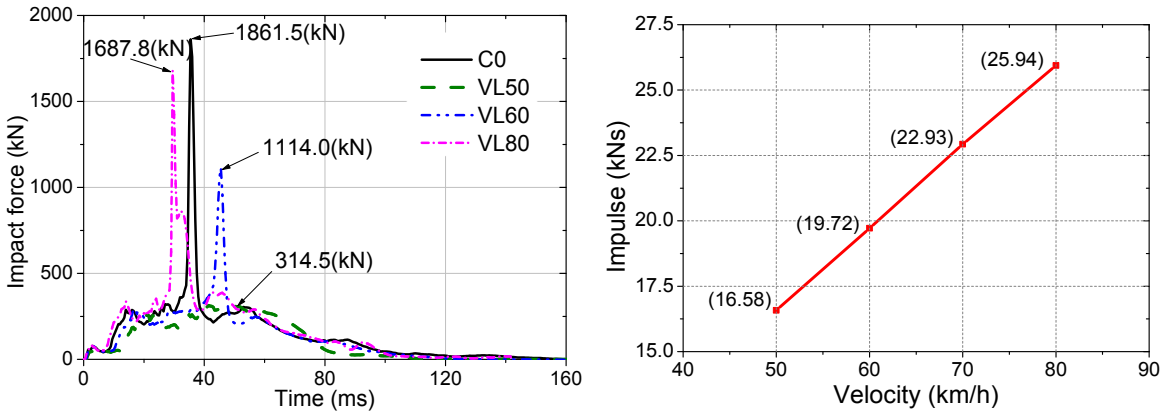

(a) Impact force time histories (b) Impulse versus velocity

Fig. 24. Impact force time history of PCSC subjected to vehicle impact with four different velocities

Figs. 25 and 26a respectively present the plastic strain contours of impacted segment and lateral displacement at the top of column under different impact velocities. More local concrete damage and higher residual displacement are observed in the columns impacted by vehicle with higher impact energy. The column freely vibrates around its original position with very small concrete damage at the impact area when the velocity is 50 km/h (VL50) (see Fig. 26) while Column VL80 exhibits severe local concrete damage and very high residual displacement (about 55 mm). The prestress load time histories of tendons under varied impact velocities are shown in Fig 26b. The column impacted with higher velocity shows larger increase in the prestress force. The increment in prestress force of column corresponding to the 50 km/h impact is 6.5% compared to the initial prestress force and they are about 10.5%, 14.0%, and 22.5% respectively for the impact velocities of 60km/h, 70km/h and 80km/h.

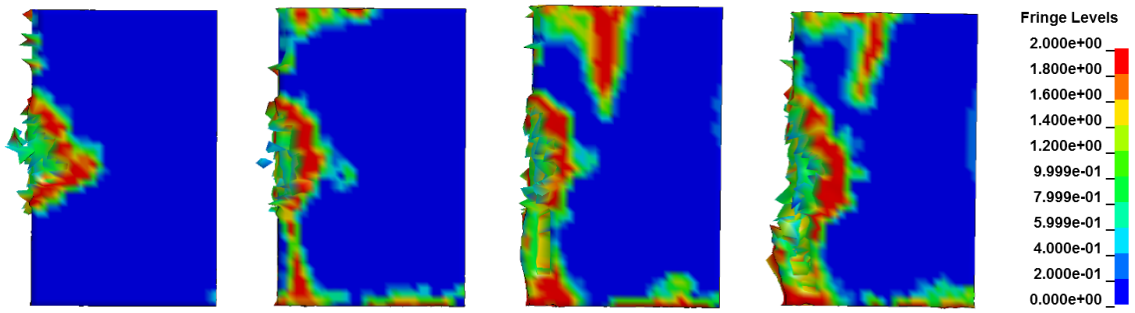

(VL50) (VL60) (C0) (VL80)

Fig. 25. Plastic strain of impacted segments with varied impact velocities

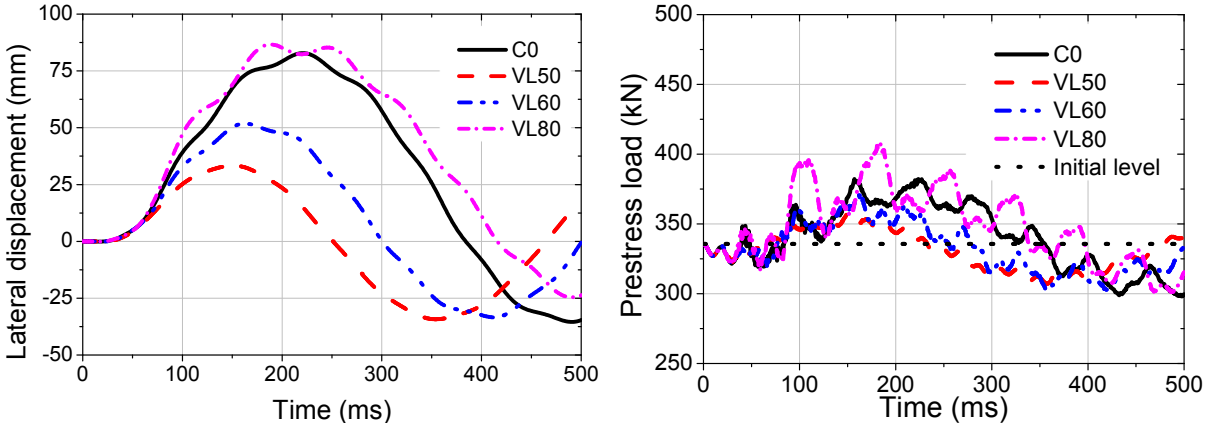

(a) Top displacement time histories (b) Prestress load time histories

Fig. 26. Column response to vehicle impact with different impact energies

4. *Conclusions*

In this study, the dynamic responses of PCSCs with un-bonded tendons subjected to vehicle collision have been numerically investigated. The accuracy of the numerical model was verified by the experimental testing results. The influences of different parameters on the performances of PCSCs are examined. The findings are summarized as follows:

1) The relative shear slips between the concrete segments and the lateral displacement of the whole column significantly decrease when the prestress force on segmental columns increases, but its effect on the impact force is negligible. On the other hand, combined with the impact

711 force, large prestress could lead to crush damage of the base segment. Therefore the prestress
712 level needs be determined through careful analysis;

713 2) The stress increase of a tendon during an impact event needs to be taken into consideration
714 to maintain the safe working condition. An increase of the prestress force in the tendon by more
715 than 20% was observed when the column is impacted by the vehicle with velocity of 80 km/h.

716 3) The columns with fewer concrete segments show better self – centering capability and
717 smaller lateral displacement. However, the number of segments in a column has minimum
718 influence on the impact force, but affects the damage mode to the concrete segment and the
719 column. The height-to-depth ratio of a concrete segment should be smaller than 2 to mitigate
720 the bending damage of the impacted segment.

721 4) The change of concrete strength shows unnoticeable effects on the residual displacement of
722 the PCSCs but it considerably affects the failure modes of the segmental column. It may also
723 affect the impact force if the concrete strength is so low such that excessive damage to concrete
724 occurs upon collision of the vehicle bumper before the collision of vehicle engine with the
725 column.

726 Due to the shear slippage between the plain concrete segments in the present study, the use of
727 shear keys on segmental columns under vehicle collision is recommended to mitigate the
728 residual displacement of the columns and increase the serviceability of the columns. The
729 application of tower concrete shear keys with reinforcements or steel tube shear keys at the
730 critical sections, i.e. the column base and the segment joint which closes to an impact point is
731 suggested in order to minimize the compression damage of the concrete material. Moreover,
732 the use of steel tubes or PVC tubes between tendons and concrete segments are recommended
733 to avoid the damage of the concrete under high vehicle impact load.

734 ***Acknowledgement***

735 The authors would like to acknowledge Australian Research Council (ARC) (DP 150104346)
736 for financially supporting this project. The first author also acknowledges the Curtin University
737 of Technology for the full Ph.D. scholarship to undertake his Ph.D. study.

738 ***References***

739 [1] Dawood HMMM. Seismic behavior and design of segmental precast post-tensioned:
740 Washington State University; 2010.
741 [2] Ou Y-C. Precast segmental post-tensioned concrete bridge columns for seismic regions:
742 State University of New York at Buffalo; 2007.
743 [3] Chung CH, Lee J, Gil JH. Structural performance evaluation of a precast prefabricated
744 bridge column under vehicle impact loading. Structure and Infrastructure Engineering.
745 2014;10:777-91.
746 [4] Zhang X, Hao H, Li C. Experimental investigation of the response of precast segmental
747 columns subjected to impact loading. Int J Impact Eng. 2016;95:105-24.
748 [5] Zhang X, Hao H, Li C. The effect of concrete shear key on the performance of segmental
749 columns subjected to impact loading. Advances in Structural Engineering.
750 2016:1369433216650210.
751 [6] Buth CE, Williams WF, Brackin MS, Lord D, Geedipally SR, Abu-Odeh AY. Analysis of
752 large truck collisions with bridge piers: phase 1. Report of guidelines for designing bridge piers
753 and abutments for vehicle collisions. Texas Transportation Institution, College Station, Texas;
754 2010.
755 [7] Bu Z-Y, Ou Y-C, Song J-W, Lee GC. Hysteretic Modeling of Unbonded Posttensioned
756 Precast Segmental Bridge Columns with Circular Section Based on Cyclic Loading Test. J
757 Bridge Eng. 2016;21:04016016.
758 [8] Sideris P, Aref AJ, Filiatrault A. Large-scale seismic testing of a hybrid sliding-rocking
759 posttensioned segmental bridge system. J Struct Eng. 2014;140:04014025.
760 [9] Motaref S, Saiidi MS, Sanders D. Shake table studies of energy-dissipating segmental bridge
761 columns. J Bridge Eng. 2013;19:186-99.
762 [10] Chou C-C, Chang H-J, Hewes JT. Two-plastic-hinge and two dimensional finite element
763 models for post-tensioned precast concrete segmental bridge columns. Eng Struct.
764 2013;46:205-17.
765 [11] Dawood H, Elgawady M, Hewes J. Factors affecting the seismic behavior of segmental
766 precast bridge columns. Frontiers of Structural and Civil Engineering. 2014;8:388-98.
767 [12] Hao H, Zhang X, Li C, Do TV. Impact response and mitigation of precast concrete
768 segmental columns. 12th International Conference on Shock and Impact Loads on Structures.
769 Singapore 2017.
770 [13] LS-DYNA L. Keyword user's manual. Livermore Software Technology Corporation.
771 2007.
772 [14] Li J, Hao H, Wu C. Numerical study of precast segmental column under blast loads. Eng
773 Struct. 2017;134:125-37.
774 [15] Chen W, Hao H, Chen S. Numerical analysis of prestressed reinforced concrete beam
775 subjected to blast loading. Mater Design. 2015;65:662-74.
776 [16] Jiang H, Chorzepa MG. An effective numerical simulation methodology to predict the
777 impact response of pre-stressed concrete members. Eng Fail Anal. 2015;55:63-78.
778 [17] Nakalswamy KK. Experimental and numerical analysis of structures with bolted joints
779 subjected to impact load: University of Nevada, USA; 2010.
780 [18] Papageorgiou A, Gantes C. Modal damping ratios for irregular in height concrete/steel
781 structures. I II III IV. 2008;6.
782 [19] Hesam P, Irfanoglu A, Hacker T. Estimating Effective Viscous Damping and Restoring
783 Force in Reinforced Concrete Buildings. Dynamics of Civil Structures, Volume 2: Springer;
784 2016. p. 265-73.

[20] Hesameddin PK, Irfanoglu A, Hacker T. Effective Viscous Damping Ratio in Seismic Response of Reinforced Concrete Structures.
[21] Pham TM, Hao H. Plastic hinges and inertia forces in RC beams under impact loads. Int J Impact Eng. 2017;103:1-11.
[22] Pham TM, Hao H. Effect of the plastic hinge and boundary conditions on the impact behavior of reinforced concrete beams. Int J Impact Eng. 2017;102:74-85.
[23] Li J, Hao H. Influence of brittle shear damage on accuracy of the two-step method in prediction of structural response to blast loads. Int J Impact Eng. 2013;54:217-31.
[24] Li J, Hao H. Numerical study of concrete spall damage to blast loads. Int J Impact Eng. 2014;68:41-55.
[25] Code C-FM. Design Code 1993 Thomas Telford London. UK; 1990.
[26] Malvar L, Crawford J. Dynamic increase factors for steel reinforcing bars [C]. 28th DDESB Seminar Orlando, USA1998.
[27] Malvar LJ, Crawford JE. Dynamic increase factors for concrete. DTIC Document; 1998.
[28] Ngo TD. Behaviour of high strength concrete subject to impulsive loading: University of Melbourne, Australia; 2005.
[29] Hao Y, Hao H, Jiang GP, Zhou Y. Experimental confirmation of some factors influencing dynamic concrete compressive strengths in high-speed impact tests. Cement and Concrete Research. 2013;52:63-70.
[30] Hao H, Hao Y, Li J, Chen W. Review of the current practices in blast-resistant analysis and design of concrete structures. Advances in Structural Engineering. 2016;19:1193-223.
[31] Hao Y, Hao H. Influence of the concrete DIF model on the numerical predictions of RC wall responses to blast loadings. Eng Struct. 2014;73:24-38.
[32] Dogan F, Hadavinia H, Donchev T, Bhonge PS. Delamination of impacted composite structures by cohesive zone interface elements and tiebreak contact. Central European Journal of Engineering. 2012;2:612-26.
[33] Sha Y, Hao H. Laboratory tests and numerical simulations of barge impact on circular reinforced concrete piers. Eng Struct. 2013;46:593-605.
[34] Center NCA. https://www.nhtsa.gov/crash-simulation-vehicle-models#12086: National Highway Traffic Safety Administration; 2016, 20 Nov
[35] AASHTO-LRFD. LRFD bridge design specifications. Washington, DC: American Association of State Highway and Transportation Officials. 2012.
[36] Fujikake K, Li B, Soeun S. Impact response of reinforced concrete beam and its analytical evaluation. J Struct Eng. 2009;135:938-50.